Spring 5-31-1994

Derivation of respiration from electrocardiogram during heart rate variability studies

Lingeng Zhao
New Jersey Institute of Technology

Copyright Warning & Restrictions

The copyright law of the United States (Title 17, United States Code) governs the making of photocopies or other reproductions of copyrighted material.

Under certain conditions specified in the law, libraries and archives are authorized to furnish a photocopy or other reproduction. One of these specified conditions is that the photocopy or reproduction is not to be "used for any purpose other than private study, scholarship, or research." If a, user makes a request for, or later uses, a photocopy or reproduction for purposes in excess of "fair use" that user may be liable for copyright infringement,

This institution reserves the right to refuse to accept a copying order if, in its judgment, fulfillment of the order would involve violation of copyright law.

Please Note: The author retains the copyright while the New Jersey Institute of Technology reserves the right to distribute this thesis or dissertation

Printing note: If you do not wish to print this page, then select "Pages from: first page # to: last page #" on the print dialog screen

ABSTRACT

DERIVATION OF RESPIRATION FROM ELECTROCARDIOGRAM DURING HEART RATE VARIABILITY STUDIES

by
Lingeng Zhao

A method was developed to derive the respiration signal from the ECG signal based on the observation that the body-surface ECG is influenced by electrode motion relative to the heart and that fluctuations in the mean cardiac electrical axis accompany respiration. S-Plus programs were developed to calculate the changes in the value of the mean cardiac electrical axis during respiration from a two lead ECG signal and to generate a continuous ECG-derived respiratory signal from the angle information.

Data were taken from 9 healthy subjects during rest, paced breathing and exercise. The respiration was derived from the recorded ECG signals. The ECG-derived respiration was compared with the original respiration recorded through an impedance pneumography device. The derived respiration shows an excellent correspondence with the original respiration. Statistical analysis indicates that the ECG-derived respiration has a high correlation with the original respiration in the frequency domain.

Our study provides a method to obtain the respiration from the ECG signal when respiration information is not directly available. This can be done either directly or from a Holter recording. It is therefore possible to do spectral analysis of heart rate variability and determine the frequency of the spectral peak occurring at the respiration frequency.

DERIVATION OF RESPIRATION FROM ELECTROCARDIOGRAM DURING HEART RATE VARIABILITY STUDIES

by
Lingeng Zhao

A Thesis
Submitted to the Faculty of
New Jersey Institute of Technology
in Partial Fulfillment of the Requirements for the Degree of
Master of Science in Biomedical Engineering

Biomedical Engineering Committee

May 1994

APPROVAL PAGE

DERIVATION OF RESPIRATION FROM ELECTROCARDIOGRAM DURING HEART RATE VARIABILITY STUDIES

Lingeng Zhao

Dr. Stanley S. Reisman, Thesis Advisor — Date
Professor of Electrical Engineering and Associate
Chairperson for Graduate Studies, NJIT

Dr. David Kristol, Committee Member — Date
Professor of Chemistry and Director of
Biomedical Engineering Program, NJIT

Dr. Thomas W. Findley, Committee Member — Date
Associate Professor of Medicine, UMDNJ
Director of Research, Kessler Institute for
Rehabilitation

BIOGRAPHICAL SKETCH

Author: Lingeng Zhao

Degree: Master of Science in Biomedical Engineering

Date: May 1994

Undergraduate and Graduate Education:

- Master of Science in Biomedical Engineering
  New Jersey Institute of Technology, Newark, NJ, 1994
- Master of Science in Biomedical Engineering
  Chinese Academy of Medical Sciences, Beijing, P. R. China, 1987
- Bachelor of Science in Electrical Engineering
  Tsinghua University, Beijing, P. R. China, 1983

Major: Biomedical Engineering

This thesis is dedicated to my wife
Qun Li
and
my parents

ACKNOWLEDGMENT

The author wishes to express his sincere gratitude to his advisor, Professor Stanley S. Reisman, for his guidance, friendship and moral support throughout this research. Special thanks to Dr. David Kristol and Dr. Thomas W. Findley for serving as members of the committee.

The author appreciates the help and suggestions from Dr. Ronald De Meersman.

TABLE OF CONTENTS

TABLE OF CONTENTS
(Continued)

Chapter **Page**

LIST OF TABLES

Table **Page**

LIST OF FIGURES

LIST OF FIGURES
(continued)

Figure **Page**

CHAPTER 1

BACKGROUND

1.1 Heart Rate Variability

The experiments on "animal electricity" conducted by Galavni and Volta two centuries ago led to the discovery that electrical phenomena were involved in the spontaneous contractions of the heart. The activation of cardiac muscle is propagated at a very rapid rate and in an orderly manner. The process of the depolarization of the cardiac muscle originates in the sinoatrial (SA) node, which is situated in the wall of the right atrium near the entrance of the superior vena cava. The cells of the SA node are autorhythmic. Because of this capability, the SA node is designated as a pacemaker. However, all areas of the heart muscle have the potential ability to serve in this capacity, but they assume this role only under abnormal circumstances. From the SA node, the process of depolarization spreads radially throughout the atria along ordinary atrial myocardial fibers and is taken over by the atrioventricular (AV) node, which is located near the top of the ventricular septum. The AV node in turn activates the bundle of His which divides into two branches serving the right and left ventricles. Through these branches the stimulus finally passes to the ventricles and generates ventricular contraction[1].

The electrocardiogram (ECG) reflects the changes over time of the electrical potential between pairs of points on the skin surface. The cardiac impulse progresses through the heart in an extremely complex three-dimensional pattern. Hence, the precise configuration of the ECG varies from individual to individual, and in any given individual

the pattern varies with the anatomical location of the leads. In general, the pattern consists of P, QRS, and T waves (Figure 1.1). They represent atrial depolarization, ventricular depolarization, and ventricular repolarization, respectively.

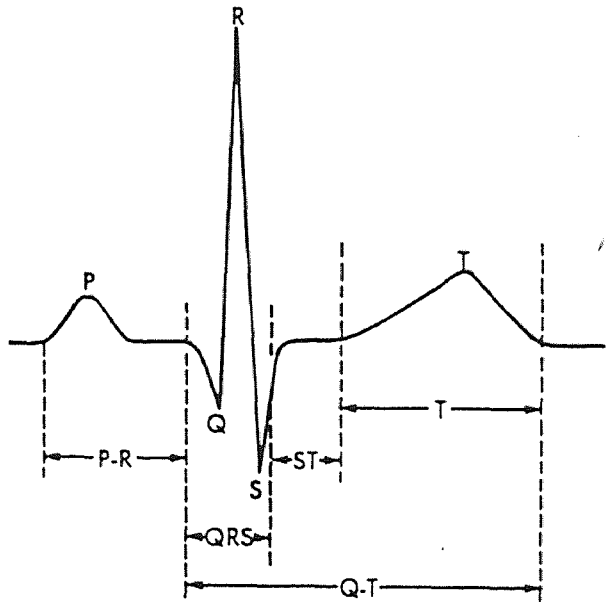

Figure 1.1 Configuration of a typical scalar electrocardiogram, illustrating the important deflections and intervals.

The SA node is usually under the tonic influence of both divisions of the autonomic nervous system. The sympathetic system enhances automaticity, whereas the parasympathetic system inhibits it. Changes in heart rate usually involve a reciprocal action of the two divisions of the autonomic nervous system. Thus an increased heart rate is produced by a diminution of parasympathetic activity (also called vagal tone) and concomitant increase in sympathetic activity; deceleration is usually achieved by the opposite mechanisms. Under certain conditions the heart rate may change by selective action of just one division of the autonomic nervous system, rather than by reciprocal changes in both divisions. For instance, during paced respiration, the heart rate is

decreased by the increase of parasympathetic activity. Ordinarily, in healthy, resting individuals parasympathetic tone is predominant. In normal adults the average heart rate at rest is approximately 70 beats per minute. During sleep the heart rate diminishes by 10 to 20 beats per minute, but during emotional excitement or muscular activity it may accelerate to rates considerably above 100. In well-trained athletes at rest the rate is usually only 50 to 60 beats per minute[2].

It has been known that healthy individuals have heart rates that fluctuate considerably even at rest, whereas decreased variability and accentuated periodicities are associated with disease[3]. Recent evidence suggests that heart rate variability is also a biologic marker of the aging process; specifically, HRV diminishes with aging. On the other hand, this loss can be attenuated by habitual exercise over time[4]. Therefore, in recent years the assessment of heart rate variability has attracted a growing interest.

1.2 Current Research in Power Spectral Analysis of Heart Rate Variability

At rest, spontaneous oscillatory fluctuations occur in blood pressure and heart rate. The study of such behavior may help to elucidate the neural control of the circulation from the point of view of basic physiology and to suggest possible clinical applications. The observed oscillatory behavior is believed to result from the interplay of feedback mechanisms involved in physiological control and the concept of interacting oscillatory systems in homeostasis is now well established[5]. The application of computer processing has facilitated the use of the techniques of systems analysis to study such interactions on a beat-by-beat basis. Variations in heart rate have been studied by deriving a heart rate variability signal, i.e. a continuous variable corresponding to the instantaneous

heart rate. It is possible to quantify the relationship between changes in cardiac rhythm and other cardiorespiratory variables using conventional methods of signal processing such as power spectral analysis.

Power spectral analysis is a process that begins by transforming a signal from the time domain to the frequency domain. Periodic functions can be represented as a sum of sines and cosines at a fundamental frequency and its harmonics. This sum is called a Fourier series. When a function is non-periodic, components may be present at all frequencies. The Fourier series is expanded to a Fourier Transform to accommodate non-periodic functions. Using Fourier transform techniques, the frequency components of the non-periodic function are found.

In power spectral analysis of heart rate variability, an interbeat interval (IBI) signal is generated by computing the time difference between successive R waves. The IBI signal must be interpolated to form an equidistant time series. Then, the heartbeat interval spectrum is generated by taking the Fourier transform of this IBI signal. Only through the transformation of these time event series to the frequency domain can the existence of physiological rhythms oscillating at specific frequencies be appreciated.

Kitney and co-workers[6] analyzed the frequency content of heart rate variability by measuring their power spectrum. In this pioneering work, they showed that in addition to the well-known fluctuations in heart rate associated with the respiratory cycle, there are also periodic fluctuations in heart rate occurring at lower frequencies (Figure 1.2). Accordingly, the power spectrum of the heart rate fluctuations contains not only a peak centered at the respiratory frequency but also peaks at two lower frequencies. Their work suggests that the low-frequency peak is related to cyclic fluctuations in peripheral

vasomotor control associated with thermoregulation, whereas the mid-frequency peak is related to the frequency response of the baroreceptor reflex, and that the blood pressure is regulated by the baroreceptors the through autonomic nervous system.

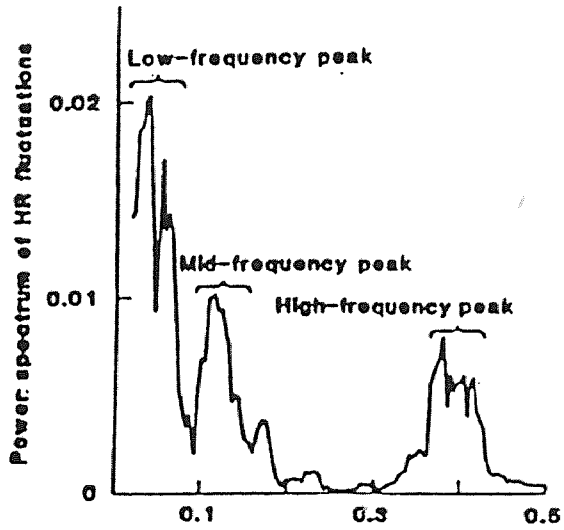

Figure 1.2 Power spectrum of heart rate fluctuations, indicating low-frequency, mid-frequency, and high-frequency peaks.

For some time there has been a tendency attempting to identify spectral peaks in predefined ranges in power spectral analysis of heart rate variability. In this method, the heart rate spectrum is divided into three frequency bands. A low-frequency band below 0.05 Hz is correlated with vasomotor control and/or temperature control. A mid-frequency band ranging from 0.06 to 0.15 Hz is associated with baroreceptor-mediated blood pressure control. A high-frequency band ranging from 0.15 to 0.4 Hz has been linked with respiration[7][8].

In 1992, Bigger, et al. using a similar method analyzed 24-hour Holter ECG data from 867 myocardial infarction patients in order to establish the association between mortality and several frequency domain measures of heart rate variability[9]. They

computed the 24-hour power spectral density and calculated the power within four frequency bands: 1) < 0.0033 Hz, ultra low frequency (ULF) power; 2) 0.0033 to < 0.04 Hz, very low frequency (VLF) power; 3) 0.04 to < 0.15 Hz, low frequency power; and 4) 0.15 to 0.4 Hz, high frequency power as the pure measure of the modulation of parasympathetic tone by respiratory frequency and depth. They also calculated the total power (power in the band, =<0.4 Hz) and the ratio of LF to HF power as a measure of the sympathovagal balance. Therefore, the mortality risk predictors were calculated by means of Cox proportional hazards analyses based on the six measurement of power spectrum density.

It has been known for more than one century that there is a influence of respiratory variation on heart rate, so-called respiratory sinus arrhythmia (RSA). RSA is a rhythmical fluctuation in heart periods at the respiratory frequency that is characterized by a shortening and lengthening of heart periods in a phase relationship with inspiration and expiration, respectively[10]. RSA is mediated by vagal nerve. RSA is being used increasingly as a measure of vagal control of the heart in psychophysiological studies. In power spectral analysis of heart rate variability, the best-known and best-defined peak reflects changes in interbeat interval that cycles up and down at the same frequency as respiration. This respiration peak corresponds approximately to the RSA, and it is purely parasympathetic in origin[11]. However, the frequencies of spontaneous respiration are not limited to within the narrow band (0.15-0.4 Hz); they can spread over a wider range of 0.05 to 0.66 Hz. The normal respiration rate can be as low as only 3 breaths per minute (0.05Hz) at rest and as high as up to 40 breaths per minute (0.66Hz) during intense exercise[12]. The following experimental results obtained at the Kessler Institute

for Rehabilitation show how incorrect the conclusions would be if only the information within the high frequency band of the heart rate spectrum is considered as the vagal activity. Figure 1.3 (a) shows the spectra of heart rate (solid line) and respiration (dashed line) of a normal subject in a resting test. The vagal peak in the heart rate spectrum is a good match to the respiration peak but both are located at 0.09 Hz, indicating that this subject has a respiration rate less than 6 breaths per minute at rest. Figure 1.3 (b) shows the result of a normal subject exercising at a level of four times resting metabolic rate. Both the respiration and vagal tone peaks are located higher than 0.5 Hz. Therefore, if for these two examples, the power were calculated within the frequency band of 0.15 to 0.4 Hz as the measure of vagal tone activity, the results would be completely wrong.

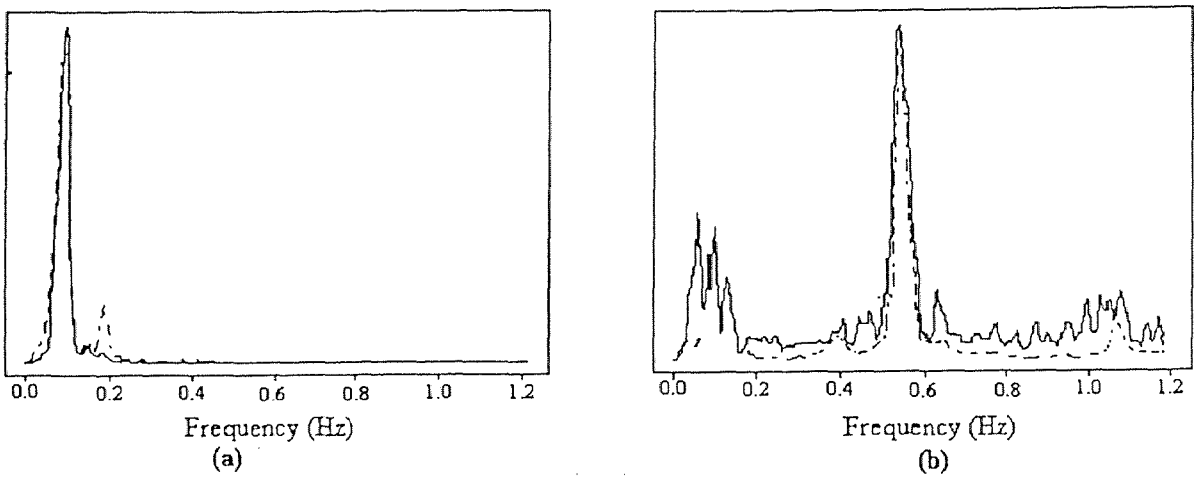

Figure 1.3 Heart rate and respiration spectra from two normal subjects. (a): resting test; (b): a test of exercise at 4 metabolic rate. The vagal tone and heart rate spectra peaks are all out of the high frequency band (0.15 to 0.4 Hz) in (a) and (b).

Zhang, Reisman, and Tapp proposed a new approach to study the heart rate variability by treating heart rate as a system of homogeneous, self-sustained oscillators perturbed by respiration through the autonomic nervous system[18]. They investigated the

mechanisms underlying cardiac timing and the interaction of heart rate with respiration by means of phase response curves. Phase shift was defined as the difference between real-time R-R interval T and natural period T_0 , normalized by T_0. The stimulus was defined as the increment of respiration amplitude at each coupling interval. The phase response curve (PRC) is the phase shift versus coupling interval. A paced breathing experiment has been completed in normal subjects and patients with chronic fatigue syndrome. Their results show that the phase response curve can predict the entrainment behavior of heart rate interacting with respiration cycles. There is a large difference in the phase response curve between the normal and abnormal PRC. Although study of phase has provided much important information, it is not complete without examining the relationship between phase shift and the increment of respiration amplitude.

Power spectral analysis of heart rate variability is a valuable tool through which neurocardiac function can be assessed non-invasively. However, its usefulness is greatly limited when the respiration signal is not available. In order to inspect the behavior of the heart; i.e., the output of the self-sustained oscillating system, the respiration; i.e., the input of the system, has to be taken into consideration. Figure 1.4 shows some experimental results of heart rate variability studies performed at the Kessler Institute for Rehabilitation. Figures 1.4 (a) and (b) show the interbeat interval spectrum (solid line) and the respiration spectrum (dashed line) for a normal subject and a stroke patient respectively. In Figure 1.4 (a) the high frequency peak of the interbeat interval spectrum is superimposed with the respiration spectrum peak, indicating that the heart rate is well regulated by the parasympathetic activity. In Figure 1.4 (b), the vagal peak is not at the same frequency as the dominant respiration spectral peak. This example clearly indicates

that without the respiration as reference, this decoupling could not be observed and the interbeat interval spectrum peak would be incorrectly assumed to be at the respiration frequency.

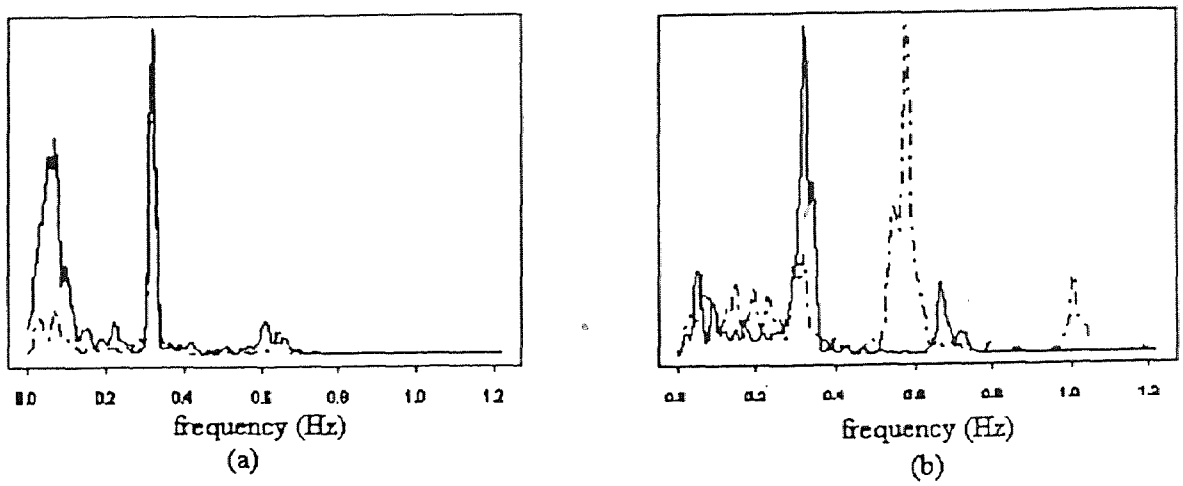

Figure 1.4 Heart rate and respiration spectra from (a): a normal subject; (b): a stroke patient. The two spectral peaks are superimposed in (a); whereas, decoupled in (b).

1.3 The Present Research

For some time there has been growing attention to the techniques dedicated to clinical signal monitoring of ambulatory patients. For example, after surviving a stroke, patients were frequently monitored by a Holter recorder during their normal life in order to record their cardiovascular system function. However, the monitoring in ambulatory subjects respiration suffers from the lack of suitable monitoring methods. As the development proceeds of power spectral analysis of heart rate variability, more and more ECG data taken from ambulatory subjects are processed in order to obtain the neurocardiac control information in health and in disease during normal life throughout the day. Since the respiration information is absent, the vagal tone is not obtainable because the respiration

frequency of the vagal tone peak can not be determined. Therefore, the neurocardiac control mechanism can not be assessed in a confident manner.

Due to the above mentioned drawbacks, we studied a method to derive the respiration signal from the ECG signal based on the well-known observation[20] that the body-surface ECG is influenced by electrode motion relative to the heart and that fluctuations in the mean cardiac electrical axis accompany respiration.

1.4 Cardiac Electrical Vector

The resting cardiac cell, like any other cell of excitable tissues (skeletal muscle, smooth muscle, nerve) maintains the separation of charged particles (ions) across its membrane. Positively charged particles (positive ions) are lined up along the outside of the membrane and negatively charged particles (negative ions) along the inside. Spontaneously, or by an external electrical stimulus, the cardiac fiber membrane becomes immediately and readily permeable to sodium ions, which therefore pass into the cell and convert its interior negative potential into a positive one; in other words, the potential of the interior of the cell exceeds that of the exterior by about 20mV. This phenomenon is called depolarization and the potential difference occurring, due to depolarization of the cell, is called an action potential (Figure 1.5). Each cardiac muscle fiber behaves as an electric dipole which has a positive and a negative terminal. During every cardiac cycle, all cardiac muscle fibers depolarize and repolarize at a very rapid rate and in an orderly manner. By summing up these dipoles generated by all cardiac cells, the resultant dipole is obtained, which represents the total electrical activity of the heart[1].

The human body, by virtue of the chemical nature of its tissue fluids, is

essentially a volume conductor (i.e., a medium that permits the conduction of electricity in three dimensions), with the boundary being limited by the body surface. Thus, when the current dipole originates in the heart it sets up an electrical field at the body surface, and potential variations within this field are easily measured.

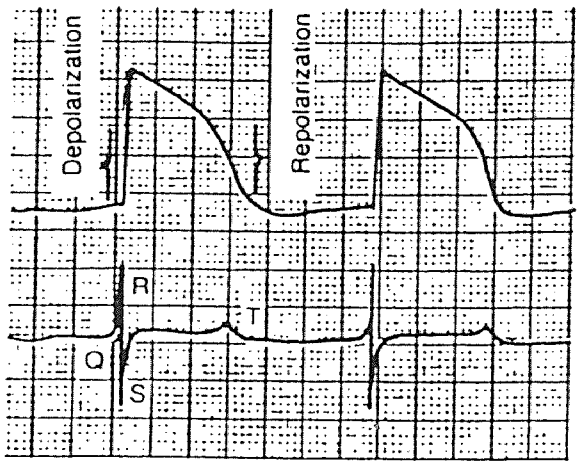

Figure 1.5 Cardiac muscle action potential. Above: monophasic action potential from a ventricular muscle fiber during normal cardiac function. Below: electrocardiogram recorded simultaneously.

In a volume conductor, the paths taken by the current depend upon the structure and geometry of the volume conductor. When the volume conductor is homogeneous, isotropic, infinitely large (in comparison to the dipole) and the dipole is located centrally, then the distribution of currents and potentials is symmetrical and obeys the simple law for the voltage induced at a distant point by a dipole.

According to this law, the electrical potential at any point P in a volume conductor is

$$Vp=\mu\cos\theta/d^2 \qquad (1.1)$$

where μ is the dipole moment (equal to the product of the charge and the length of the dipole), d is the distance from the point P to the center of the dipole, and θ is the angle between the dipole axis and the line to that distant point P[1] (Fig. 1.6). Thus the potential varies inversely with the square of the distance and is dependent upon the angle that the line from the dipole to the point P makes with respect to the axis of the dipole.

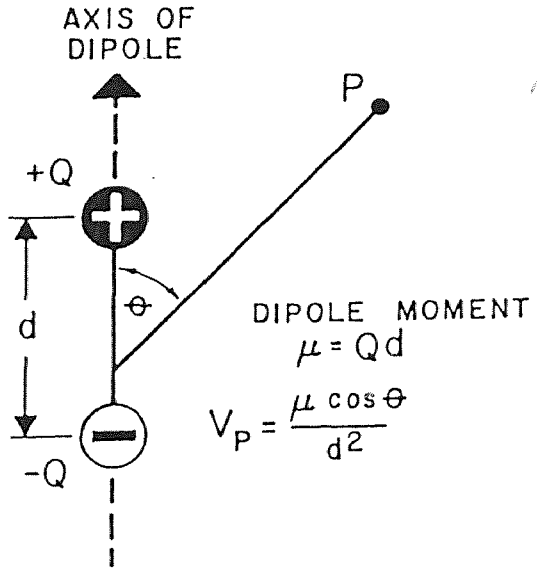

Figure 1.6 Pictorial representation of the law governing the voltage induced by a dipole at a distant point P.

The human body, however, is an inhomogeneous, anisotropic, finite-sized and irregular-shaped volume conductor and the heart dipole is located eccentrically. But, in practice this inhomogeneity seems to be rather unimportant except perhaps for the low resistance and consequent short-circuiting effect of blood within the heart cavities. That short-circuiting effect of blood within the heart presumably diminishes the effect of all the separate sources and leads to a unification of electrical activity, which lends further support to the hypothesis that the heart behaves as a single dipole.

The cardiac dipole, generated by the working heart, has a certain direction from

- to +, and a certain magnitude and thus can be represented as a vector. This vector, the so-called heart vector, is oriented in the direction of the dipole axis and has magnitude proportional to the dipole moment.

The origin of the heart vector is assumed to be in the center of the heart mass and to remain in this location throughout the single cardiac cycle. The direction and magnitude of this vector changes from moment to moment in the course of a single cardiac cycle. Consequently, the changes of this vector form a continuous loop in a 3-dimensional space and this loop is called the spatial vectorcardiogram as shown in Figure 1.7.

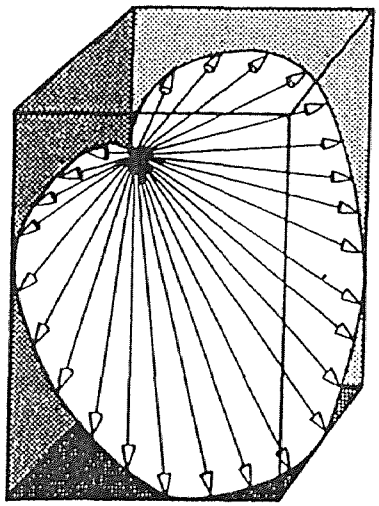

Figure 1.7 Instantaneous heart vectors. The spatial vector loop is formed by the termini of an infinite number of instantaneous heart vector.

The spatial vectorcardiogram consists of 3 successive loops, namely: the "P loop", the "QRS loop", and the "T loop". The P loop represents the time course of all instantaneous vectors produced during atrial depolarization. The QRS loop represents the time course of all instantaneous vectors produced during ventricular depolarization. The

T loop represents the time course of all instantaneous vectors produced during ventricular repolarization (Figure. 1.8).

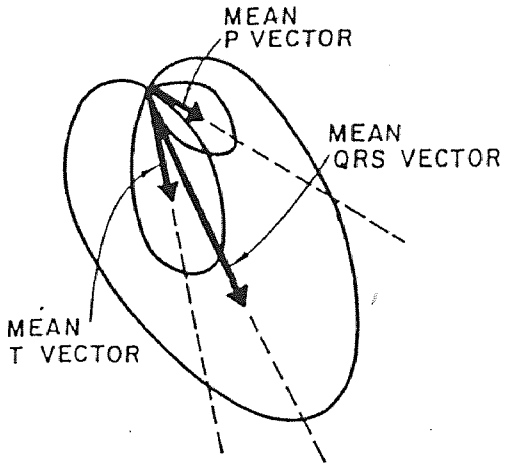

Figure 1.8 The mean P, QRS, and T vectors in the frontal plane.

The electrical activity of the heart at any moment of a cardiac cycle is represented by a single dipole which subsequently is depicted as an instantaneous heart vector. For the whole cardiac cycle there are an infinite number of instantaneous heart vectors. At each subsequent instant during the cardiac cycle, with different regions of the ventricles becoming depolarized, the resultant dipole for each instant has a different magnitude and direction. Several instantaneous vectors may be replaced by one mean, or resultant vector, which is obtained by summation of these instantaneous vectors. From the mathematical point of view there is a difference between the mean and resultant vectors in the sense that although they have the same direction, the mean vector may have different magnitude because it is obtained by dividing the sum of the n instantaneous vectors by the number of vectors. Figure 1.8 shows the three mean P, QRS, and T vectors resulting from the instantaneous vectors during each cardiac cycle.

Electrocardiographic deflections recorded in a given lead reflect the magnitude and direction of the particular heart spatial vector as it is projected on this lead axis. The amplitude of the electrocardiographic deflection is thus determined by the magnitude of the heart spatial vector, as well as by the angle between this vector and a given lead axis. Polarity of the electrocardiographic deflection depends on how the particular heart vector projects on the lead axis. If the particular heart vector projects onto the negative side of the lead axis, a negative deflection is recorded in this lead. Since the ECG deflections represent the projection of the heart vector on a given lead axis, the direction and magnitude of the cardiac spatial vector are read from the ECG deflection.

Figure 1.9 shows the electrocardiogram from the standard bipolar limb leads[22]. In lead I, the negative terminal of the electrocardiograph is connected to the right arm and the positive terminal to the left arm. In lead II, the negative terminal is connected to the right arm and the positive terminal to the left leg. In lead III, the negative terminal is connected to the left arm and the positive terminal to the left leg. The reference point (ground) is connected to the right leg.

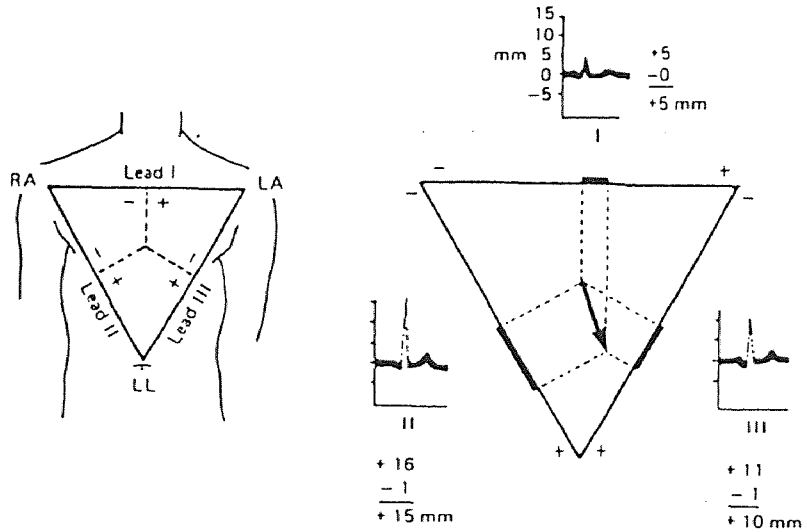

Figure 1.9 Standard bipolar limb leads of electrocardiogram.

CHAPTER 2

METHODS

2.1 ECG Signals Containing Respiration Information

A biological signal mainly determined by a specific biological system is often influenced by other interacting systems. Therefore, it is possible to derive a respiratory signal from an ECG signal, which is mainly determined by a non-respiratory system but partly influenced by the respiratory system.

ECG signals recorded from the surface of the chest are influenced by motion of the electrodes with respect to the heart, and by changes in the electrical impedance of the thoracic cavity. The expansion and contraction of the chest which accompanies respiration result in motion of the chest electrodes. In clinical practice, the existence of a conspicuous amplitude modulation in an ECG tracing is often observed as indicated in Figure 2.1. In terms of the equivalent dipole model of cardiac electrical activity,

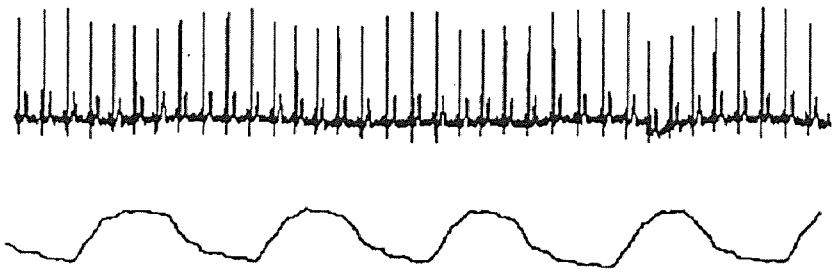

Figure 2.1 Respiration-induced modulation of QRS amplitude. Upper trace: ECG; lower trace: respiration measured by a impedance pneumography device.

respiration could induce a modulation in the direction and the amplitude of the mean

cardiac electrical vector. It is possible to measure a fluctuation in the mean cardiac electrical axis in order to obtain a derived respiration signal. The determination of the way in which the ECG tracings can be examined to obtain a significant respiratory signal is an open problem for which the published literature give no solution.

In 1985, Pinciroli began studying methods for determining the direction of the axis, in order to create "virtual ECG leads", which would represent what might be obtained from electrodes fixed in position relative to the heart[19]. Moody, et al., derived respiration from body-surface ECG signals by calculating the fluctuations in mean cardiac electrical axis and applied the technique in successfully monitoring sleep apnea patients[20][21]. However, we have not seen reports on the application of the ECG-derived respiratory signal in power spectral analysis of heart rate variability.

It has been noted in the preceding discussions that the vector of current flow through the heart changes rapidly as the impulse spreads through the myocardium. It changes in two respects: First, the vector increases and decrease in length because of the increasing and decreasing voltage of the vector. Second, the vector changes its direction because of changes in the average direction of the electrical potential of the heart. The vectorcardiogram depicts these changes in the vectors at the different times during the cardiac cycle, as illustrated in Figure 2.2[12]. Intuitively, this concept is easily acceptable: the axis of the cardiac electrical vector points out the prevalent direction of heart electrical activity.

In the vectorcardiogram of Figure 2.2, point 5 is the zero reference point, and this point is the negative end of all the vectors. While the heart is quiescent, the positive end of the vector also remains at the zero point because there is no electrical potential.

However, as soon as current begins to flow through the heart, the positive end of the vector leaves the zero reference point.

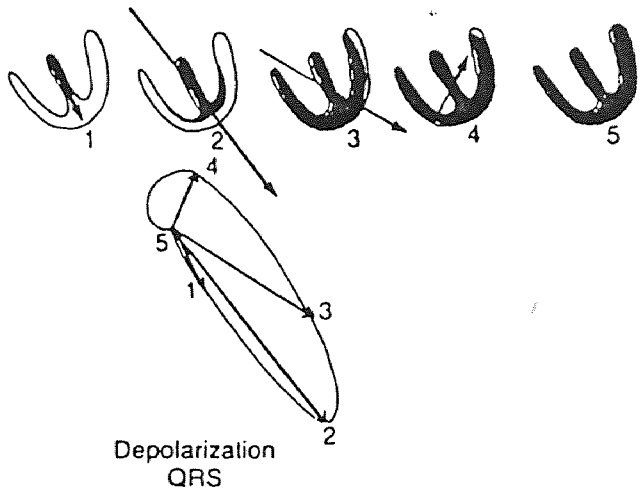

Figure 2.2 The QRS vectorcardiogram.

When the septum first becomes depolarized, the vector extends downward toward the apex of the heart, but it is relatively weak, thus generating the first portion of the vectorcardiogram, as illustrated by the positive end of vector 1. As more of the heart becomes depolarized, the vector becomes stronger and stronger, usually swinging slightly to one side. Thus, vector 2 of Figure 2.2. represents the state of depolarization of the heart about 0.02 seconds after vector 1. After another 0.02 seconds, vector 3 represents the potential of the heart , and vector 4 occurs in yet another 0.01 second. Finally, the heart becomes totally depolarized, and the vector becomes zero once again, as shown at point 5. The elliptical figure generated by the positive ends of the vectors is called the QRS vectorcardiogram.

Clinically, the electrical axis of the heart is usually determined from the standard bipolar limb lead electrocardiograms rather than from the vectorcardiogram. Figure 2.3

illustrates a method for doing this. After recording the standard leads, one determines the maximum potential and polarity of the recording in two of the leads. To determine the actual vector of the ventricular mean electrical potential, one draws perpendicular lines from the apices of the two net potentials of leads I and III, respectively. Leads I and III are chosen because their axes are truly orthogonal. The point of intersection of these two perpendicular lines represents, by vectorial analysis, the apex of the actual mean QRS vector in the ventricles, and the point of intersection of the two lead axes represents the negative end of the actual vector. Therefore, the mean QRS vector is drawn between these points. The approximate average potential generated by the ventricles during depolarization is represented by the length of the vector, and the mean electrical axis is represented by the direction of the vector. Thus, the orientation of the mean electrical axis of the normal ventricles is determined as in Figure 2.3.

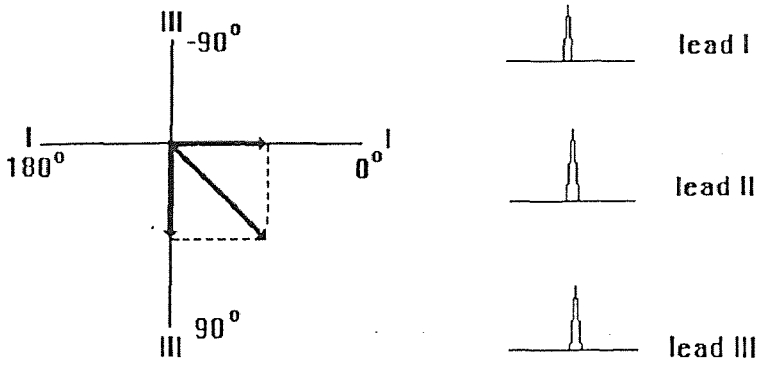

Figure 2.3 Plotting the mean electrical axis of the heart from two electrocardiographic leads.

The influence of respiration to body surface ECG signals can also be shown in Figure 2.4 . In time period t_1, the subject was asked to do a deep inhalation and hold. In time period t_2, the subject was asked to do a deep exhalation and hold. During inhalation

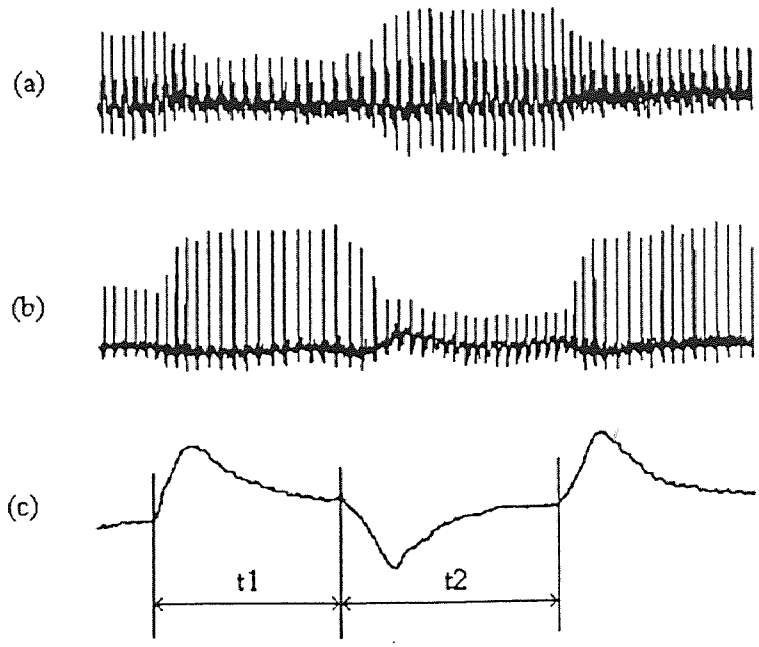

Figure 2.4 Different lead ECG signals influenced by respiration. (a): lead I ECG; (b): lead III ECG: (c) respiration; t1: deep inhalation and hold; t2; deep exhalation and hold.

and hold, the amplitude of lead I is decreased and that of lead III increased significantly. During exhalation and hold, the amplitude of lead I is increased and that of lead III decreased greatly. Speculatively this observation can be explained that during inhalation the apex of the heart is stretched towards the abdomen due to the filling of the lungs and diaphragm moving inferiorly and during exhalation the apex of the heart is compressed towards the chest due to the emptying of the lungs and diaphragm moving superiorly. Due to the anatomical changes of the heart in the chest during respiration, the angles of the mean QRS vector vary within a range as shown in Figure 2.5, which causes the amplitude changes in leads I and III.

In our study, the area of each normal QRS complex in each of two leads was measured over a fixed time window. Since the window width was fixed, the area was

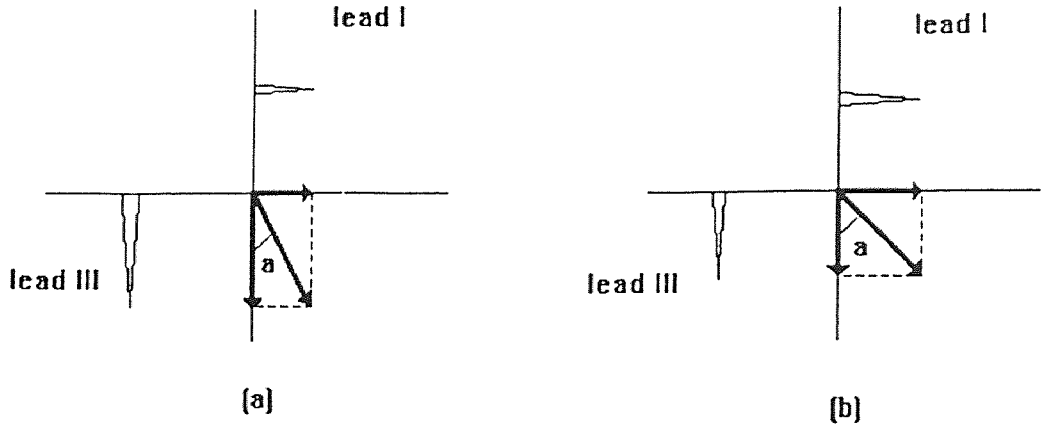

Figure 2.5 Axis of the mean QRS vector influenced by respiration. α: the angle of the axis respect to the lead III axis. (a): deep inhalation and hold; (b): deep exhalation and hold.

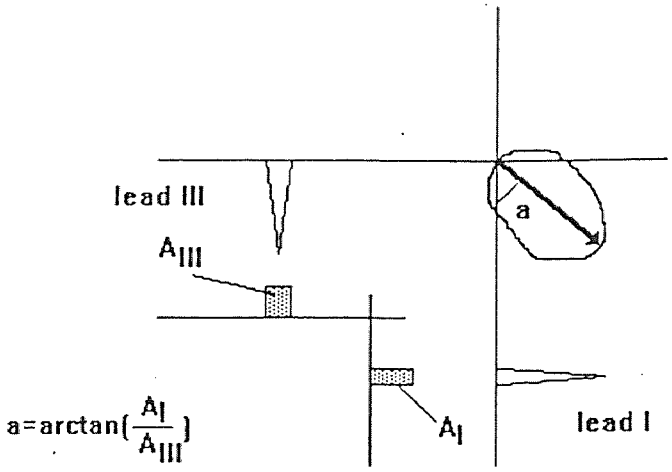

Figure 2.6 Calculating the direction of the mean QRS vector axis. A_I: area for QRS complex in lead I; A_{III}: area for QRS complex in lead III; α: the angle of the mean QRS vector axis respect to lead III axis.

proportional to the amplitude of the ECG signal, hence to the projection of the mean cardiac electrical vector on the lead axis (Figure 2.6). Assuming that the leads are orthogonal, the arctangent of the ratio of the areas measured in the two leads yields the angle of the mean axis of QRS vector with respect to one of the lead axes. The angle values were interpolated to produce a continuous ECG-derived respiratory signal.

2.2 Instrumentation

ECG signals were recorded using a Quinton Q4000 Stress Test Monitor/Controller (Quinton Instrument, Co., Seattle, WA). The output signals from the monitor were acquired by a IBM-compatible 386/40 MHz data acquisition computer at a 200Hz sampling rate. The data acquisition computer had a Keithley Metrabyte Das-16 analog/digital interface board installed. In order to compare the ECG-derived respiratory signals with the real respiration, a respiration wave was recorded simultaneously by an impedance pneumography device (RESPI, UFI, Morrow Bay, CA) and also digitized by the data acquisition computer at the same sampling rate. The impedance pneumography device recorded the respiration wave indirectly by means of electric impedance plethysmography. A constant high frequency current was applied to the chest and the resulting voltage reflecting the impedance changes due to the filling and emptying of the lungs during respiration was detected. The software program used to control the data acquisition was Streamer by Keithley, version 3.25.

2.3 Experimental Setup

Since our purpose was to derive the respiratory signal from the ECG signal and use it in the application of power spectral analysis of heart rate variability, the experimental protocol followed the routine experimental protocol designed in the investigation of heart rate variability for stroke survivors performed at the Kessler Institute for Rehabilitation.

Two leads ECG signals (lead I and III) and the respiration wave were collected on healthy subjects during eight 2-minute test conditions: 1) resting, non-paced breathing

(used to determine 1 MET VO_2/ml/kg body weight level; 2) resting, paced breathing at a rate of 8 breaths per minute (bpm); 3) resting, paced breathing at 12 bpm; 4) resting, paced breathing at 18 bpm; 5) exercising at 2 METS; 6) exercising at 3 METS; 7) exercising at 4 METS; and 9) resting, normal relaxed breathing, immediately following exercise (recovery).

2.4 Data Analysis

The ECG and respiration data analysis was performed on an IBM-compatible 486/50 MHz computer. The data analysis software package used was S-Plus for windows V3.1 (Statistical Sciences, Seattle WA), which includes modern statistical techniques and permits writing of custom S-Plus programs.

In S-Plus, the ECG signals were detrended by using a locally weighted robust regression procedure and R peaks were detected by a previously developed signal processing software algorithm. In order to form the ECG-derived respiration signal, the following processes were performed. See the Appendix B and C for details on derivation procedures and S-Plus programming.

2.4.1 PQ Junction Detection

S-Plus software was written to detect the PQ junction. The algorithm is explained in Figure 2.7. Based on the position of each R peak, a time period ac was set backward from the R peak. Within the time period ac, the minimum value b was detected as the point of the PQ junction.

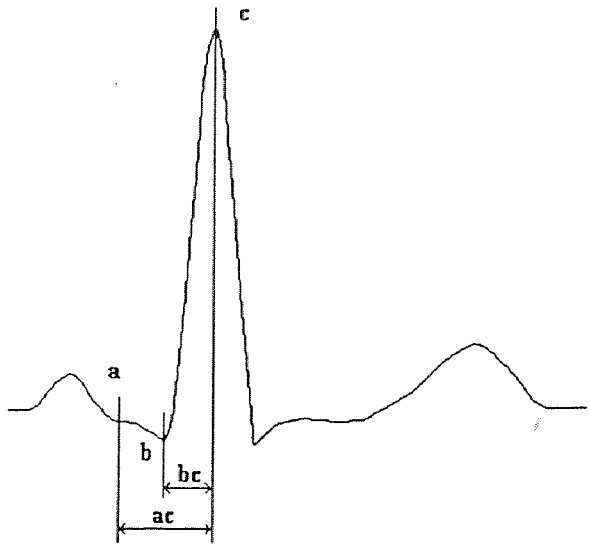

Figure 2.7 PQ junction detection algorithm.

2.4.2 Determination of Time Window Width

After all PQ junctions were detected, the average length between the PQ junction and the R peak was calculated. We defined a time window width determined by a ratio of the average length between PQ junction and R peak as given in the following equation:

$$W=k\Sigma L_{qr}(i)/n \qquad (2.1)$$

Where W: time window width

L_{qr}: time interval between Q and R

n: number of QRS complex

k: constant

See section 4.3 for details on determination of the k.

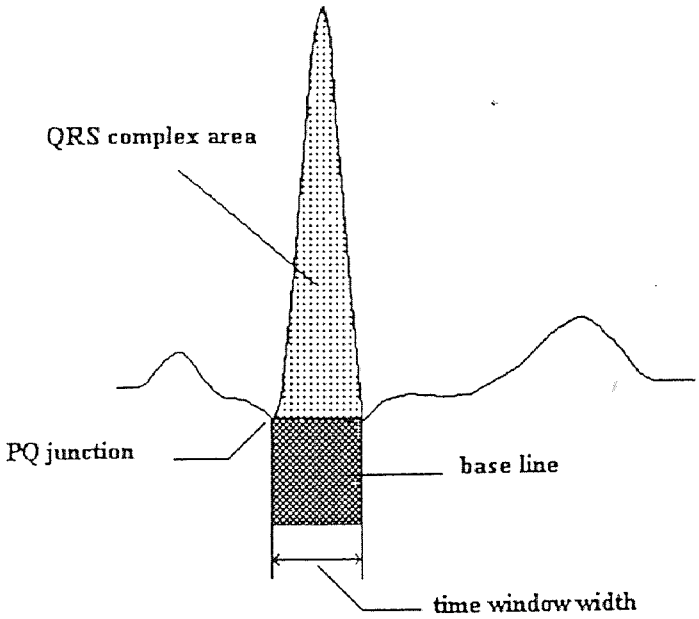

Figure 2.8 Computing QRS complex area.

2.4.3 QRS Complex Area Calculation

After subtracting the base line (the area within the time window below the PQ junction), the area under each QRS complex within the time window was calculated (Figure 2.8) and an area function was generated from each ECG signal (Figure 2.9 (c) and (d)). In order to rule out the influence of bad R peak and/or PQ junction detection, the area data was examined visually. The outliers (ranging from 0 to 10%) were removed and the R peaks corresponding to the outliers were detected manually. This procedure might be performed several times until all QRS complex areas were calculated confidently.

2.4.4 Generation of ECG-Derived Respiration

Figure 2.9 (c) shows the angle values of the mean electrical axis of the QRS vector

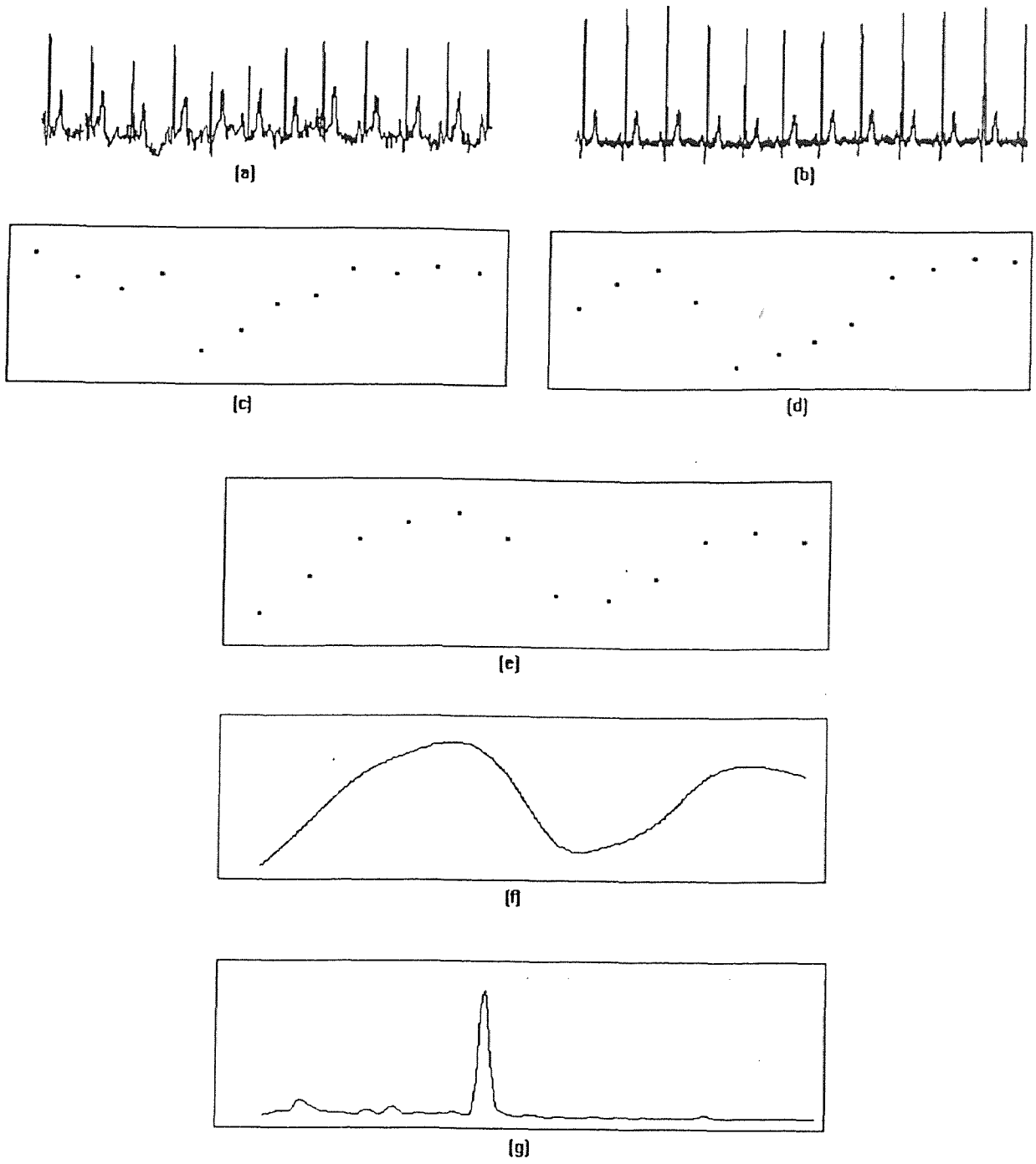

Figure 2.9 Procedures of deriving respiration from ECG signals. (a) lead I ECG; (b) lead III ECG: (c) QRS complex areas from (a); (d) QRS complex areas from (b); (e) angle values of the axis of the QRS vector calculated from (c) and (d); (f) ECG derived respiration by interpolating (e); (g) spectrum of the ECG-derived respiration.

calculated based on the area data computed from the leads I and III ECG signals in the following formula:

$$\alpha[i]=\arctan(A_I[i]/A_{III}[i]) \qquad (2.2)$$

where $\alpha[i]$: angle value of the mean electrical axis of the ith QRS vector

$A_I[i]$: area value of the ith QRS complex in lead I

$A_{III}[i]$: area value of the ith QRS complex in lead III

To produce a continuous ECG-derived respiration signal, the angle values were interpolated by a cubic spline approximation (Figure 2.9 (f)). Since we are interested in the spectrum of the derived respiration signal, the FFT was applied to the signal (Figure 2.9 (g)). In order to compare the ECG derived respiration signal to the original respiration signal recorded from the impedance pneumograph, the FFT was also applied to the latter.

Our method to derive respiration from ECG signals is basically the same in theory as Moody and coworkers'[20][21]. However, they did not specify the lead configuration and did not present their software. Therefore, the work was an original investigation into optimum lead configuration as well as original software development. Also, Moody, et al. did not utilize derived respiration in heart rate variability studies and did not consider studies involving exercise where the body motion could have affected the derivation of respiration.

CHAPTER 3

RESULTS

3.1 Visual Comparison

Figure 3.1 in Appendix A shows the data from one normal subject and processed by the method described in the previous chapter. There are four graphs from each test. For example, in Figure 3.1 (a) (data from the resting test), the upper left graph is a two minute sample of the original respiration signal recorded from the impedance pneumography device; the upper right graph is the spectrum of the original respiration; the lower left graph is the ECG-derived respiration signal, the lower right graph is the spectrum of the ECG-derived respiration. The respiration signals both from recording and derivation are arranged in the same column on the left and their spectra in the same column on the right so as they can be compared easily. In Figure 3.1 (a), there are 11 respiration waves both in the original respiration signal and ECG-derived respiration signal. The ECG-derived respiration is 180 degrees out of phase with the original respiration because the signals are interpreted in the opposite way in these two conditions. Since the impedance pneumograph measures the impedance during respiration, an increase in signal amplitude represents inhalation and a decrease in signal amplitude represents exhalation. In the ECG-derived respiration, we calculated the changes in the angle of the electrical axis of the mean QRS vector using the lead III axis as reference (Figure 2.5). The angle value decreases during inspiration and increases during expiration. Although there is the difference in phase between the original respiration and the ECG-derived

respiration, it does not influence the spectra. In the right column of Figure 3.1(a), the peak of the spectrum of the ECG-derived respiration is at the same frequency as the peak in the spectrum of the original respiration. Both spectra are very similar in shape. If we examine the remainder of Figure 3.1, we find that even the derived spectra from the exercise tests (Figure 3.1 (e), (f),and (g)) have a remarkable similarity in shape with the original spectra even though the body is moving greatly during exercise.

3.2 Central Frequency Comparison

The spectrum of the ECG-derived respiration signal contains the information we are going to use in the power spectral analysis of heart rate variability. We will utilize the spectral information much more often than the time function of the derived respiration.

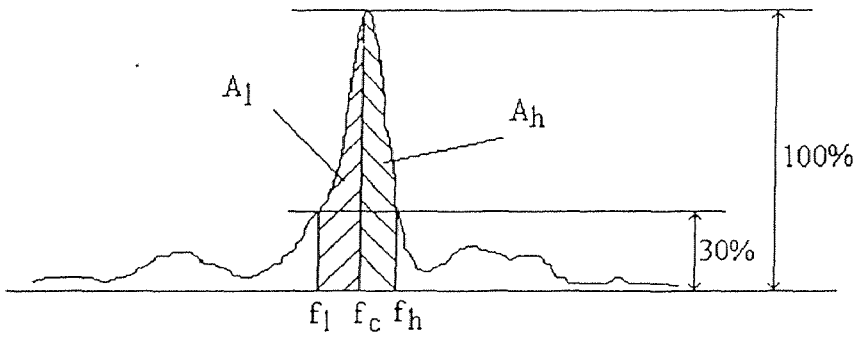

Figure 3.2 Central frequency definition. f_l: low frequency; f_h: high frequency; f_c: central frequency.

To characterize the similarity of the derived spectrum to the original spectrum quantitatively, we calculated the central frequency for both spectra. Figure 3.2 shows how the central frequency was calculated. The amplitude of the spectral peak was detected first. Then the frequency values at 30% of the spectral peak were located on both sides;

i.e. the low frequency f_l and the high frequency f_h in Figure 3.2. The central frequency f_c was computed in such a way that the area under the spectral curve between f_l and f_c was equal to the area between f_c and f_h; i.e.

$$A_l = A_h \tag{3.1}$$

where

$$A_l = \int_{fl}^{fc} S(f)\,df \tag{3.2}$$

$$A_h = \int_{fc}^{fh} S(f)\,df \tag{3.3}$$

S(f): spectral function

Table 3.1 gives the central frequency calculation results for both the original spectrum f_{co} and derived spectrum f_{cd} from 9 healthy subjects. We also listed the relative difference in between f_{co} and f_{cd} given by the following equation:

$$\text{relative difference} = (f_{co}-f_{cd})/f_{co}\times 100 \tag{3.4}$$

The first line of table 3.1 in the column corresponding to subject 1 is the central frequency of the original spectrum for the resting test. The second line in the same column shows the central frequency of the derived spectrum for the same test. The third line in the column is the relative difference between the central frequency of the original spectrum and that of the derived spectrum. If we proceed down the column, we see the central frequencies of the original and derived spectra and the relative difference for each test for the same subject. If we proceed from left to right in Table 3.1, we see the central frequency of original spectrum, the central frequency of derived spectrum and the

Table 3.1 Results of central frequency calculation (continued on next page).

Subject		1	2	3	4
rest	original (f_{co}) (Hz)	0.0903	0.2506	0.2856	0.2905
	derivation (f_{cd}) (Hz)	0.0879	0.2522	0.2881	0.3044
	relative difference	2.66	-0.64	-0.88	-4.78
paced 8 bpm	original (f_{co}) (Hz)	0.1440	0.1440	0.1449	0.1408
	derivation (f_{cd}) (Hz)	0.1432	0.1440	0.1440	0.1432
	relative difference	0.56	0.00	0.62	-1.7
paced 12 bpm	original (f_{co}) (Hz)	0.2132	0.2156	0.2124	0.2140
	derivation (f_{cd}) (Hz)	0.2132	0.2156	0.2116	0.2157
	relative difference	0.00	0.00	0.38	-0.79
paced 18 bpm	original (f_{co}) (Hz)	0.3190	0.3263	0.3174	0.3141
	derivation (f_{cd}) (Hz)	0.3190	0.3271	0.3182	0.3117
	relative difference	0.00	-0.25	-0.25	0.77
exercise 2 METs	original (f_{co})	0.1522	0.2864	0.3166	0.3239
	derivation (f_{cd}) (Hz)	0.1571	0.2856	0.3174	0.3231
	relative difference	-3.22	0.28	-0.25	0.25
exercise 3 METs	original (f_{co}) (Hz)	0.1790	0.3263	0.3174	0.3320
	derivation (f_{cd}) (Hz)	0.1839	0.3271	0.3174	0.3418
	relative difference	-2.74	-0.25	0.00	-2.95
exercise 4 METs	original (f_{co}) (Hz)	0.1961	0.4500	0.3206	----------*
	derivation (f_{cd}) (Hz)	0.1945	0.4370	0.3182	0.4232
	relative difference	0.82	2.89	0.77	----------*
recovery	original (f_{co}) (Hz)	0.1123	0.2978	0.3158	0.4354
	derivation (f_{cd}) (Hz)	0.1164	0.2954	0.3158	0.4346
	relative difference	-3.65	0.81	0.00	0.18

Table 3.1 (continued from last page)

Subject		5	6	7	8	9
rest	original (f_{co}) (Hz)	0.3011	0.2458	0.3507	0.2116	0.2563
	derivation (f_{cd}) (Hz)	0.3019	0.2507	0.3516	0.2083	0.2620
	relative difference	-0.27	-1.99	-0.26	1.56	-2.22
paced 8 bpm	original (f_{co}) (Hz)	------**	0.1473	0.1449	0.1457	0.1465
	derivation (f_{cd}) (Hz)	------**	0.1464	0.1457	0.1449	0.1465
	relative difference	------**	0.61	-0.55	0.55	0.00
paced 12 bpm	original (f_{co}) (Hz)	0.2083	0.2148	0.2148	0.2173	0.2230
	derivation (f_{cd}) (Hz)	0.2140	0.2157	0.2148	0.2173	0.2222
	relative difference	-2.74	-0.42	0.00	0.00	0.36
paced 18 bpm	original (f_{co}) (Hz)	------**	0.3215	0.3223	0.3304	0.3231
	derivation (f_{cd}) (Hz)	------**	0.3206	0.3215	0.3296	0.3223
	relative difference	------**	0.28	0.25	0.24	0.24
exercise 2 METs	original (f_{co}) (Hz)	------**	0.3068	0.3524	0.2490	0.2897
	derivation (f_{cd}) (Hz)	------**	0.3215	0.3467	0.2515	0.2889
	relative difference	------**	-4.79	1.62	-1.00	0.28
exercise 3 METs	original (f_{co}) (Hz)	0.4199	0.2661	0.3597	0.2645	0.3166
	derivation (f_{cd}) (Hz)	0.4167	0.2645	0.3580	0.2637	0.3158
	relative difference	0.76	0.60	0.47	0.30	0.25
exercise 4 METs	original (f_{co}) (Hz)	------**	0.2840	0.3752	0.3076	0.3385
	derivation (f_{cd}) (Hz)	------**	0.2987	0.3743	0.3084	0.3410
	relative difference	------**	-5.18	0.24	-0.26	-0.74
recovery	original (f_{co}) (Hz)	0.2930	0.2747	0.2330	0.2629	0.3003
	derivation (f_{cd}) (Hz)	0.2897	0.2507	0.2330	0.2629	0.3052
	relative difference	1.13	-1.33	0.00	0.00	-1.63

corresponding relative difference of each test for all subjects. Some central frequency numbers in Table 3.1 are missing. The ones marked with single asterisk are missing because the respiration was poorly recorded by the impedance pneumography device due to a bad preparation. The tests for subject 5 marked with a double asterisk were not performed.

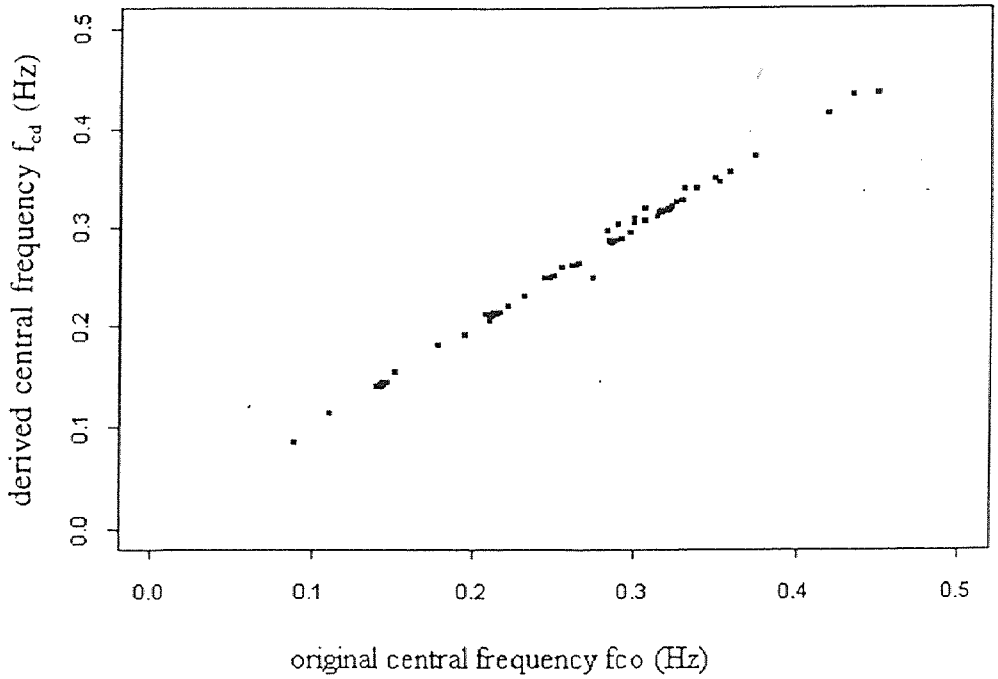

Figure 3.3 Scatter plot of the derived central frequency f_{cd} versus the original central frequency f_{co}.

Figure 3.3 plots the derived central frequency f_{cd} versus the original central frequency f_{co} as a visual check on correlation between these two variables. To analyze our results statistically, we performed correlation test and paired t-test. Before doing the tests, we used exploratory data analysis to verify if our data was outlier-free and nearly normal because the classical method of statistical inferences depend heavily on these assumptions.

Figure 3.4 shows the graphical results of the exploratory data analysis. The

variable f_{df} used here is the difference between f_{co} and f_{cd}. We can get a good picture of the shape of the distribution generating our data, and also detect the presence of outliers, by looking at the four plots in Figure 3.4.

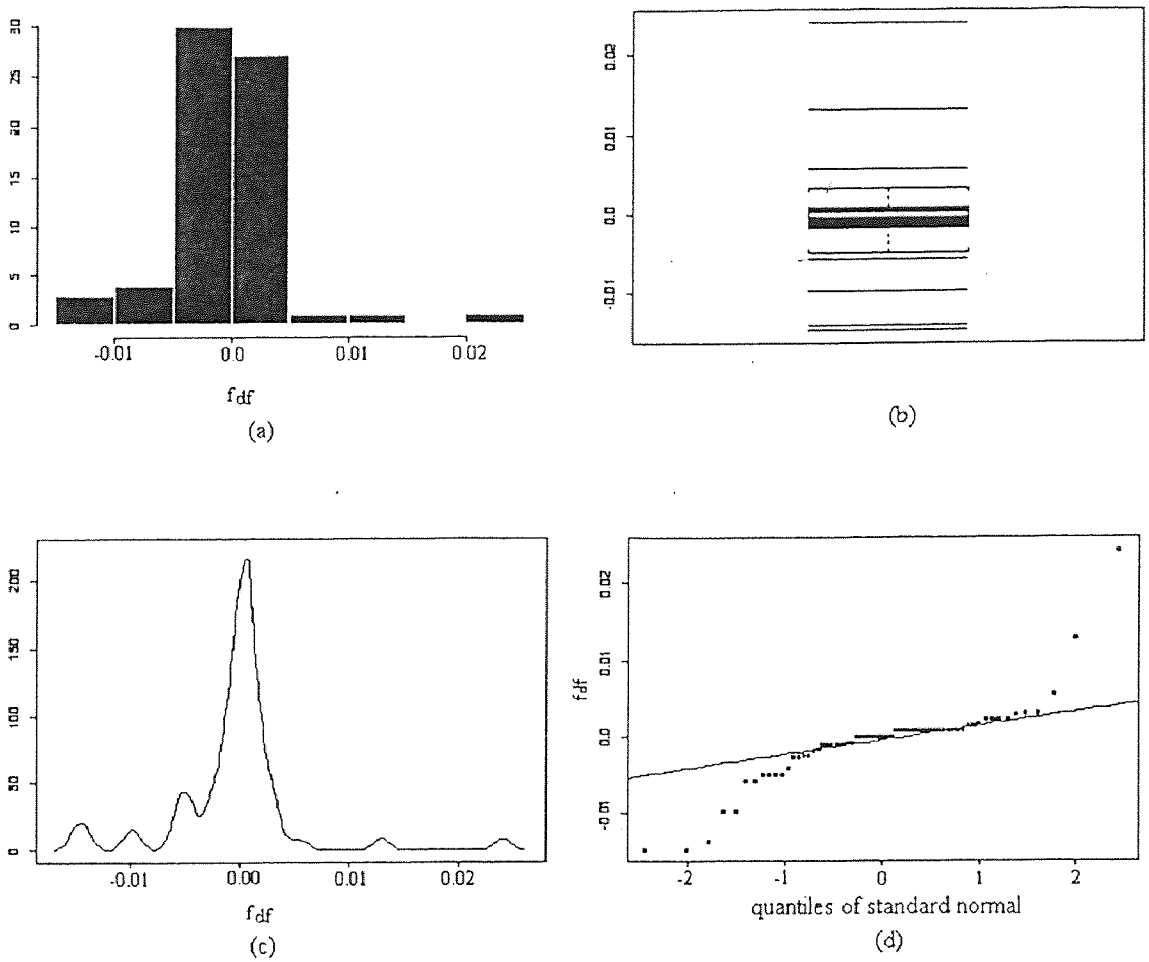

Figure 3.4 Exploratory data analysis plots for the difference between f_{co} and f_{cd}. (a) histogram; (b) box plot; (c) density plot; (d) quantile-quantile plot.

Figure 3.4 (a) and (b) are the histogram and the box plot of f_{df}. A histogram shows the number of data points that fall in each of a number of intervals. A box plot is a simple graphical representation showing the center and spread of a distribution, along with a display of unusually deviant data points, called outliers. The horizontal line in the

interior of the dark box in Figure 3.4 (b) is located at the median of the f_{df}. This estimates the center of the distribution for the data. The height of the box is equal to the interquartile distance, or IQD, which is the difference between the third quartile of the data and the first quartile. The IQD indicates the spread or width of the distribution for the data. The whiskers (the dotted lines extending from the top and bottom of the box) extend to the extreme values of the data or a distance 1.5×IQD from the center, whichever is less. Data points which fall outside the whiskers may be outliers, indicated by horizontal lines. In Figure 3.4 (b), the three lines above the whiskers and the four lines below it represent outliers.The density plot in Figure 3.4 (c) is essentially a smooth version of the histogram, which provides smooth estimates of population frequency, or the probability density curve. A quantile-quantile plot, or qqplot, is a plot of one set of quantiles against another set of quantiles. The normal qqplot in Figure 3.4 (d) consists of a plot of the ordered values of our data versus the corresponding quantiles of a standard normal distribution. If the qqplot is fairly linear, our data are reasonably Gaussian; otherwise, they are not.

Of these four plots in Figure 3.4, the histogram and density plot give us the best picture of the variable distribution shape, which is nearly normal, while the box plot and normal qqplot give the clearest display of the outliers. The box plot also gives a clear indication of the median, and the upper and lower quartiles (the upper and lower ends of the box).

The two samples used in the paired t-test and correlation test were the central frequency of the original spectrum f_{co} and that of the derived spectrum f_{cd}. The two tests were performed on the central frequencies for all tests (test one through eight) from all

subjects and on each individual test for all subjects. In the paired t-test, our null hypothesis is that the difference between the mean of the derived central frequency μ_{fcd} and the mean of the original central frequency μ_{fco} is zero. Our alternative hypothesis is $\mu_{fcd} \neq \mu_{fco}$. The test was set to give a 95% confidence interval for $\mu_{fcd} - \mu_{fco}$. Table 3.2 lists the results of the t-test and the correlation test. The first column of data shows the p values from each t-test, the second column is the 95% confidence interval for $\mu_{fcd} - \mu_{fco}$, the third column is the mean of f_{co}-f_{cd}, and the correlation coefficient from the correlation test is in the last column. From table 3.2, we can see that, except for the resting test, all p-values are significantly greater than 0.05. That means there is no difference between μ_{fcd} and μ_{fco}. The null hypothesis is actually true and the alternative hypothesis should be rejected. The intervals for $\mu_{fcd} - \mu_{fco}$ to fall in at a 95% confidence level are all very small ranges around zero. The high correlation coefficients in the table indicate that there is a high association between the derived central f_{cd} and the original central frequency f_{co}. If we carefully examine the relative difference values for the resting test listed in Table 3.1, we can find that most of the relative differences are negative numbers. This is possibly why the p-value is small (0.0783) for this group of data. If we increased the sample size, this statistical error would be overcome.

3.3 Evaluation of the Holter and Tape Player System Stability

Since our eventual goal for studying this method is to apply it to Holter data analysis, we performed experiments using a Holter recorder (CardioCorder, Model 459, Del Mar Avionics, Irvine, California). In order to use the Holter and tape player system confidently, we first examined the system stability.

Table 3.2 Results of the paired t-test and correlation test between f_{co} and f_{cd}.

	p-values	95% confidence interval	mean of f_{co} - f_{cd}	correlation coeff.
overall	0.4004	-0.001845, 0.000746	0.000549	0.9977
rest	0.0783	-0.008000, 0.000534	-0.003733	0.9980
paced at 8 bpm	0.9527	-0.000938, 0.000988	-0.000025	0.8241
paced at 12 bpm	0.2999	-0.002293, 0.00804	-0.000744	0.8681
paced at 18 bpm	0.2086	-0.000362, 0.001387	0.000512	0.9831
exercise at 2 METS	0.4138	-0.006886, 0.003186	-0.00185	0.9954
exercise at 3 METS	0.5599	-0.003939, 0.002295	-0.000822	0.9983
exercise at 4 METS	0.9964	-0.007576, 0.007547	0.000014	0.9956
recovery	0.4254	-0.004171, 0.008949	0.002388	0.9948

3.3.1 Sampling Rate Determination

To meet the need of recording a 24-hour ECG signal on an ambulatory subject, a Holter recorder is designed to have a very low recording speed (1 mm per second). After recording, a Holter tape is usually sent to a scanning company and analyzed in a specially designed expensive machine. The arrhythmia information (if there are any) recorded on the tape will be detected and an analysis report will be generated. Since we need the heart rate variability information recorded on a Holter tape, we have to analyze the tape in our laboratory.

We have found that we can recover the ECG from a Holter tape by using a consumer quality cassette player. The player available in our laboratory is a JVC TD-W10 Cassette Deck. The play back speed is about 47 mm per second. In order to obtain a 200 Hz sampling rate for the original ECG signals recorded with the Holter recorder, we had to determine the actual sampling rate when the Holter tape was played back on the cassette player.

A two-hour 60 beat per minute ECG signal generated by an ECG simulator (HEARTSIM 2000, Laerdal Medical Corp, Armonk, NY) was recorded with the Holter recorder. The signal was played back on the cassette player and acquired by the IBM-386 data acquisition computer at an initial sampling rate of 10kHz. The data was processed in S-Plus and the R peaks of the simulated ECG signal were detected. The average interbeat index number was 206.8, indicating that the initial sampling rate was too high. To sample the Holter ECG signal at 200 Hz, the final sampling rate f_s should be:

$$f_s = (200/206.8)\times 10 = 9.67 \text{ (kHz)} \qquad (3.5)$$

3.3.2 Stability Evaluation

Our next task was to evaluate the tape speed stability of the Holter recorder-cassette playback system. In order to accomplish this, we should first determine the stability of the ECG simulator. A two minute 60 beat per minute ECG signal from the simulator was acquired directly into the data acquisition computer (through an amplifier). The R peaks were detected and the interbeat index numbers were calculated. The interbeat index numbers were exact 200 except for three 201's periodically distributed among the 120 interbeat intervals. This might be caused by our relatively low sampling rate, which could cause the sampling point for the outliers to not be exactly on the peak of the R waves. Therefore we will assume that the ECG simulator has an acceptable stability.

Two 2-minute 60 beat per minute simulated ECG recorded by the Holter recorder were acquired into the data acquisition computer at a sampling rate of 9.67 kHz and processed in S-Plus. The mean of the interbeat interval (μ_{ibi}) and the interbeat interval with the biggest variation (V_{ibi}) were calculated. The relative tape speed stability was calculated as following:

$$\text{Relative stability} = [1-\text{abs}(\mu_{ibi}-V_{ibi})/\mu_{ibi}]\times 100 \qquad (3.6)$$

The average relative tape speed stability of the Holter recorder-cassette player system calculated from the two 2-minute simulated ECG samples was determined to be 99.08%.

3.4 Derived Respiration Using Holter Recording

The experimental setup was the same as discussed in section 2.2 and 2.3. except that the

ECG signals (lead I and III) were recorded on the Holter recorder rather than the Quinton Q4000 Stress Test Monitor. The tape with the recorded ECG signals was played back on the cassette tape player and acquired by the IBM-compatible 386 data acquisition computer at the sampling rate of 9.67 kHz for each data channel. The data were processed in S-Plus following the same procedure discussed in section 2.4.

Figure 3.5 in Appendix A shows the original respiration recorded from the impedance pneumography device and Holter ECG-derived respiration and their spectra from one normal subject. Although the ECG signals came from the indirect recording device and a lot more artifact might be induced through the recording and play back process, we still obtained good derived respiration and the spectral information. The derived spectra shown in Figure 3.5 have good correspondence with the original spectra.

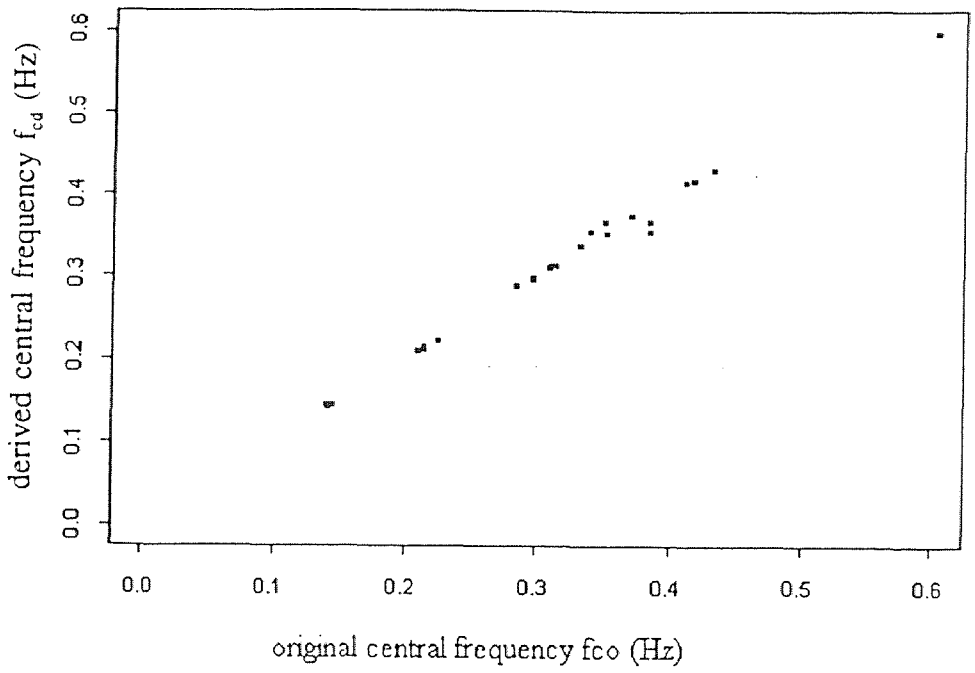

Figure 3.6 Scatter plot of the derived central frequency f_{cd} versus the original central frequency f_{co} for Holter data.

Table 3.3 Results of central frequency calculation for Holter data.

Subject		1	2	3
rest	original (f_{co}) (Hz)	0.3410	0.2987	0.2262
	derivation (f_{cd}) (Hz)	0.3548	0.2970	0.2214
	relative difference	-4.05	0.57	2.12
paced 8 bpm	original (f_{co}) (Hz)	0.1432	0.1416	0.1473
	derivation (f_{cd}) (Hz)	0.1440	0.1457	0.1473
	relative difference	-0.56	-2.90	0.00
paced 12 bpm	original (f_{co}) (Hz)	0.2108	0.2157	0.2148
	derivation (f_{cd}) (Hz)	0.2116	0.2157	0.2140
	relative difference	-0.38	0.00	0.36
paced 18 bpm	original (f_{co}) (Hz)	0.3125	0.3149	0.3109
	derivation (f_{cd}) (Hz)	0.3133	0.3141	0.3101
	relative difference	-0.25	0.25	0.26
exercise 2 METS	original (f_{co}) (Hz)	0.3329	0.6407	0.2856
	derivation (f_{cd}) (Hz)	0.3385	0.5990	0.2897
	relative difference	-1.71	0.94	-1.44
exercise 3 METS	original (f_{co}) (Hz)	0.3711	0.4134	0.3524
	derivation (f_{cd}) (Hz)	0.3752	0.4175	0.3662
	relative difference	-1.10	-0.99	-3.92
exercise 4 METS	original (f_{co}) (Hz)	0.4183	0.4346	0.3857
	derivation (f_{cd}) (Hz)	0.4199	0.4321	0.3678
	relative difference	0.38	0.58	4.64
recovery	original (f_{co}) (Hz)	0.3532	0.3849	0.2987
	derivation (f_{cd}) (Hz)	0.3532	0.3540	0.2897
	relative difference	0.00	8.03	0.00

Table 3.4 Results of the paired t-test and correlation test between f_{co} and f_{cd} for Holter data

	p-values	95% confidence interval	mean of f_{co} - f_{cd}	correlation coeff.
overall	0.7820	-0.003248, 0.004265	0.000508	0.9965
rest	0.7134	-0.027188, 0.022321	-0.002433	0.9972
paced at 8 bpm	0.3227	-0.007032, 0.003765	-0.001633	0.6846
paced at 12 bpm	0.9999	-0.001987, 0.001987	0.00	0.9684
paced at 18 bpm	0.6667	-0.002028, 0.002561	0.000266	0.9011
exercise at 2 METS	0.7382	-0.016698, 0.013955	-0.001366	0.9999
exercise at 3 METS	0.1514	-0.021245, 0.006578	-0.007333	0.9903
exercise at 4 METS	0.4017	-0.019273, 0.031806	0.006266	0.9881
recovery	0.4226	-0.034017, 0.054617	0.0103	0.9360

Table 3.3 lists the original central frequency f_{co} and derived central frequency f_{cd} and the relative difference calculated by equation 3.4 from 3 healthy subjects. Except for the recovery test from subject 2, the relative differences are all within the ±5% range.

Figure 3.6 shows the f_{cd} versus f_{co} as a visual check on correlation between the derived central frequency and the original central frequency for our Holter data.

Table 3.4 gives the paired t-test results and the correlation coefficient between f_{co} and f_{cd}.

CHAPTER 4

DISCUSSION AND CONCLUSIONS

As a tool, the power spectral analysis of heart rate variability has permitted the biomedical investigator to explore the relatively elusive autonomic nervous system in a noninvasive manner. Some recent studies indicate that power spectral analysis of heart rate variability holds a significant potential for the diagnosis of neurocardiac disorders. However, research protocols thus far have focused on establishing the association between the signal power in some fixed frequency bands and the speculated physiological origins. Due to the obvious drawbacks discussed in the previous chapters, we investigate a method to derive the respiration signal from the ECG signal based on the observation that the body-surface ECG is influenced by electrode motion relative to the heart and that fluctuations in the mean cardiac electrical axis accompany respiration.

4.1 Correlation Between f_{cd} and f_{co}

4.1.1 Non-Holter ECG-derived Respiration

Table 3.2 lists the results of the correlation test and paired t-test performed on the central frequencies of the original and derived spectra. The derived respiration was obtained from the ECG signals recorded by the Quinton Stress Test Monitor from 9 normal subjects. From Table 3.2 it can be clearly seen that the correlation coefficients are significantly high, ranging from 0.8241 to 0.9983. The overall correlation coefficient for the data from all subjects and all tests is 0.9977. This suggests that there is a strong correlation between

the central frequency of the ECG-derived respiration spectrum f_{cd} and that of the original respiration spectrum f_{co}. It indicates that our ECG-derived respiration bears a good resemblance to the original respiration recorded from the impedance pneumograph in the frequency domain. Although the respiration information recorded by means of the impedance plethysmography technique is also an indirect respiration signal, we use it as our reference throughout our study because this method gives very good results in most applications.

In Figure 3.1 in Appendix A, it can be seen that the derived respiration and their spectra show an excellent correspondence with the original respiration and spectra. From all data we analyzed, we found that the best correspondence in shape between the spectra of the derived respiration and that of the original respiration result from the paced breathing tests. The reason for this might be that the paced breathing test generates a very regular respiration signal with an essentially single frequency component. This unitary property of the paced breathing test allows a greater error tolerance for the ECG-derived respiration.

Although the derived respiration of the paced breathing tests have the best correspondence in shape with the original respiration, the correlation coefficients in Table 3.2 are relatively low for these tests. The reason for that might be that the central frequency values for both original and derived for each paced breathing test are all very close for all subjects because they all breathed at the same rate. Compared to others, these groups do not have a good straight line shape distribution as shown in Figure 4.1. However, if we look at Table 3.1, we can find that the central frequency values for the paced breathing tests have the smallest relative difference.

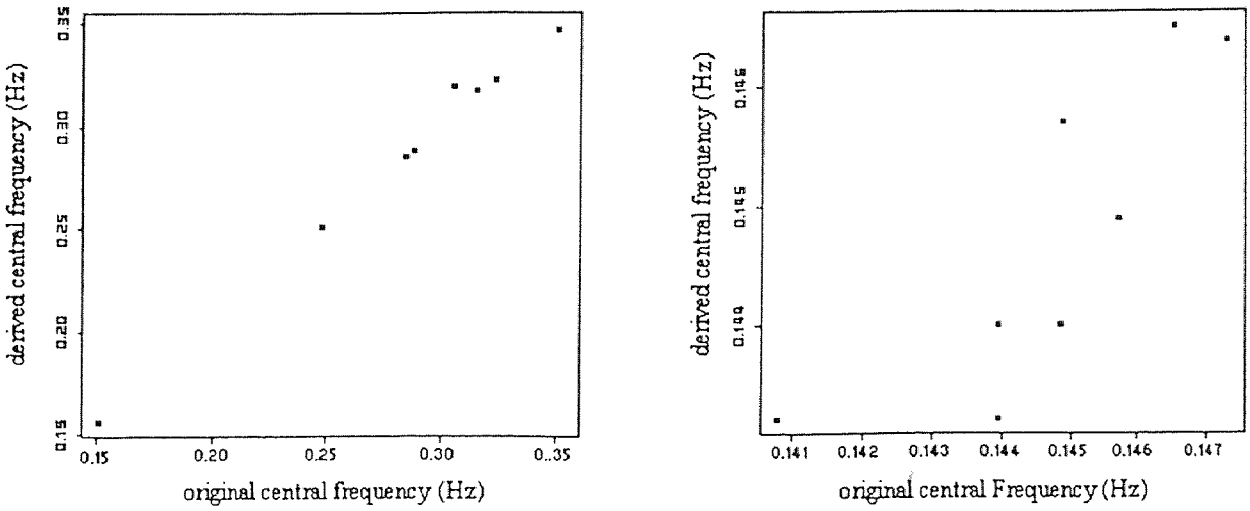

Figure 4.1 Plot of derived central frequency versus original central frequency for (a) test of exercising at 3 METS; (b) paced breathing at 8 bpm.

4.1.2 Holter ECG-derived Respiration

The frequency response of the Holter recorder is from 0.05 to 100 Hz. The tape player (JVC TD-W 10 Cassette Deck) has a frequency response of 30 to 16000 Hz, ±3dB. If all frequency components recorded by the Holter tape were output from the tape player, the requirement of the frequency response of the tape player should be from 2.5 to 5000 Hz because the play back speed is about 50 times greater than the recording speed. Since the frequency response of the tape player does not cover the required frequency band, we lose the Holter ECG information at the low frequency end. The actual frequency components of the original signal obtained from the tape player is between 0.6 and 100 Hz, which is suitable to produce an undistorted output of the original ECG signal. A cross correlation between the original and tape output signals will be performed in the future to quantify this observation.

Table 3.4 lists the results of the correlation test and paired t-test performed on the

central frequencies of the original and derived spectra for the Holter data. The correlation coefficients are still very high. The overall correlation coefficient is 0.9965, indicating a strong correlation between f_{cd} and f_{co} for the Holter data. The reason that we performed our experiments with the Holter recorder is to verify if the technique can be applied to the Holter data. We did see some small peaks on the side of the main peak in the derived spectra for the exercise and recovery tests. These might result from the mechanical instability of the tape player.

4.2 Limitations

This ECG-derived respiration technique is based on the phenomenon that respiration modulates the change in the angle of the cardiac electrical vector axis. However, from our observation, this modulation is subject dependent. It might be related to the type of respiration (abdominal versus thoracic) and the difference in the anatomical structure of each individual. Figure 4.2 shows lead I ECG signals from two healthy young female subjects in the test of paced breathing at 12 breaths per minute. In Figure 4.2 (a), the

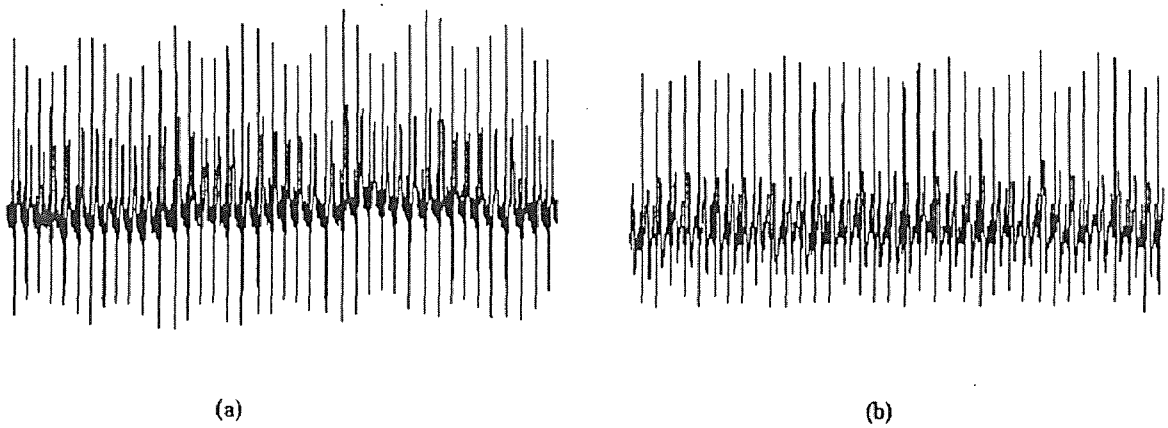

Figure 4.2 Subject dependent respiration modulated ECG signals. The respiration modulation to the ECG signal in (a) is greater than that in (b).

ECG signal amplitude is modulated by the respiration, whereas, in Figure 4.2 (b), the degree of this modulation is much smaller. The difference in the modulation might be related to tidal volume.

Of the three limb leads, lead I has the most respiration information despite having the smallest ECG signal amplitude. This is because the normal angle of the cardiac electrical vector axis is about 60° relative to the transverse plane. When respiration modulates the angle fluctuating around this value, the change of the projection of the cardiac electrical vector on the lead I axis has the biggest effect. Since we need an orthogonal lead configuration, leads I and III are the best choice.

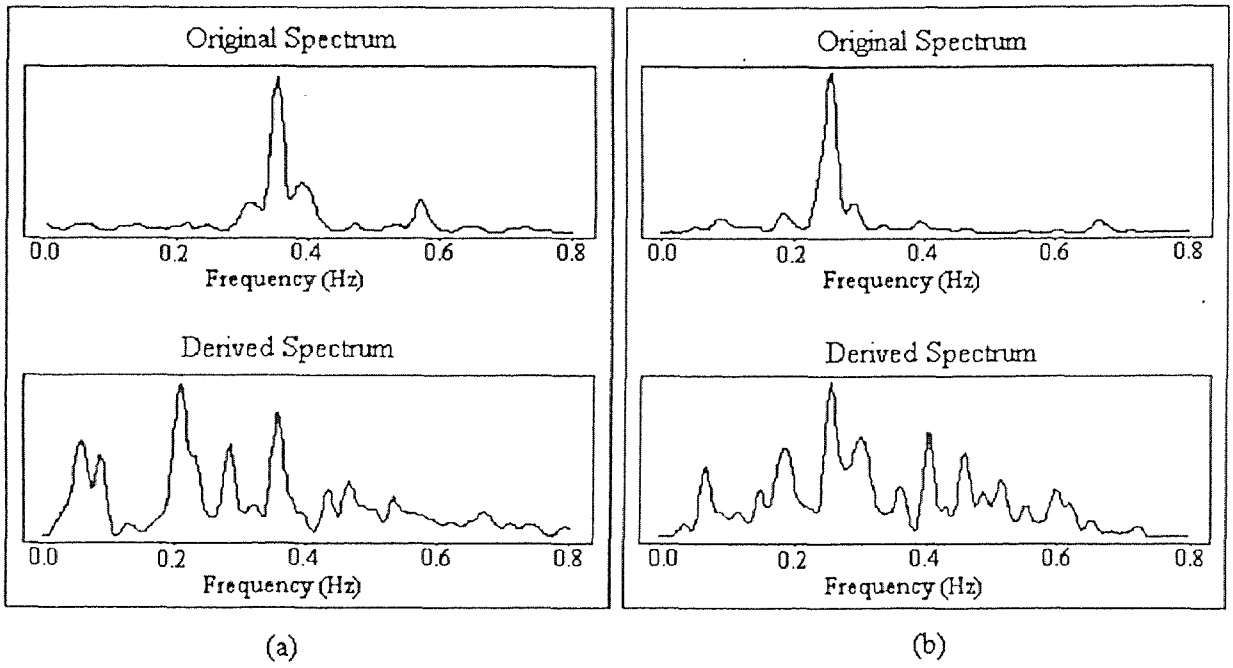

Figure 4.3 ECG-derived respiration spectra from other lead configurations. (a) from lead II ECG; (b) from a leads V1and V5 configuration.

In order to determine the optimum ECG lead configuration, we performed experiments with different configurations including one lead and two leads. Figure 4.3

shows some experimental results. In Figure 4.3 (a), the derived spectrum was from a lead II ECG signal during exercise at 3METs. Although the respiration frequency peak is present, the amplitude of the interference at the low frequency end is greater than the that of the respiration peak. Compared to lead I, lead II contains less respiration information due to its close alignment with the cardiac electrical vector. The signal to noise ratio in this case is much lower than for leads I or III. Figure 4.3 (b) shows the results of a leads V1 and V5 configuration from a resting test. The major peak of the derived spectrum is located approximately at the respiration frequency, but the derived spectrum contains relatively high noise compared to the clean original spectrum. Since leads V1 and V5 are not truly orthogonal, it is possible to induce noise and give a less accurate result.

To derive respiration from ECG signals, two conditions have to be satisfied: first, the recorded ECG signal has to contain respiration information; second, the respiration information has to be extracted correctly from the ECG signals. Because the respiration information is contained in the amplitude modulation of the recorded ECG signals, the correct respiration might not be derived reliably if the ECG signal is poorly recorded and has a very low signal to noise ratio. Speculatively, in the cases that the changes in the angle of the cardiac electrical vector are also influenced by sources besides respiration, for instance, intense exercise, the respiration signal might not be correctly obtained from the ECG signal. This can be verified by properly designing experimental protocols.

4.3 Some Key Points in The Derivation

Although the recorded ECG signal contains respiration information, without correct extraction, the information could not be obtained. There are three key steps in the

derivation of the respiration from ECG signals: 1) R peak detection; 2) PQ junction detection; 3) QRS complex area calculation. Each step directly influences the result of next step. If anything goes wrong, it is possible to get a falsely derived result.

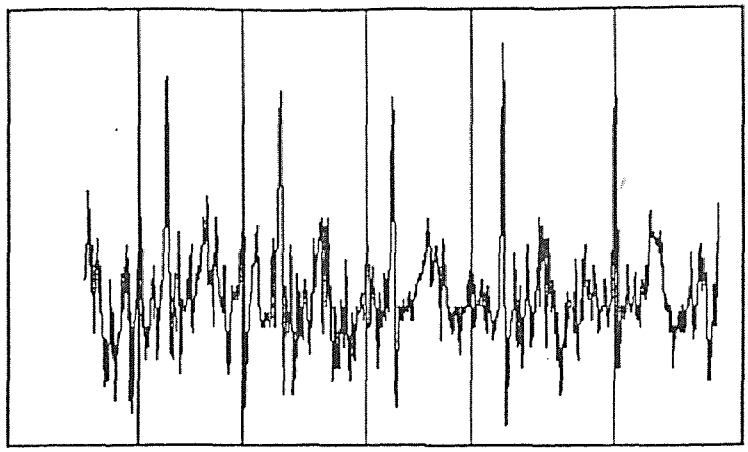

Figure 4.4 Incorrect R peak detection. The thin lines from the top to the bottom of the box indicate the detected R peaks.

Some ECG signals, especially the ones from the exercise tests, have a high artifact level due to the movement of the body and the possible relative movement between the electrode and the skin surface. Figure 4.4 shows an R peak detection result of an ECG signal containing a large amount of noise. The thin lines from the top to the bottom of the box indicate the positions of the detected R peaks. Due to the improper selection of the required parameters required for the R peak detection program, all R peaks were detected incorrectly except for the last one. In this case visual inspection of the detection result is very important. Correct R peak detection of the signals containing large noise can be obtained by repetitively selecting different values for the parameters and visually checking the detection result.

Figure 4.5 shows how correct PQ junction detection is important to the derived respiration. The ECG signal shown in Figure 4.5 (a) has high frequency noise and some spikes. If the length ac (see section 2.4.1 and Figure 2.7) were set as shown in the figure when performing the PQ junction determination, the result would be incorrect because the spike present within time period ac has the lowest value and the algorithm would choose

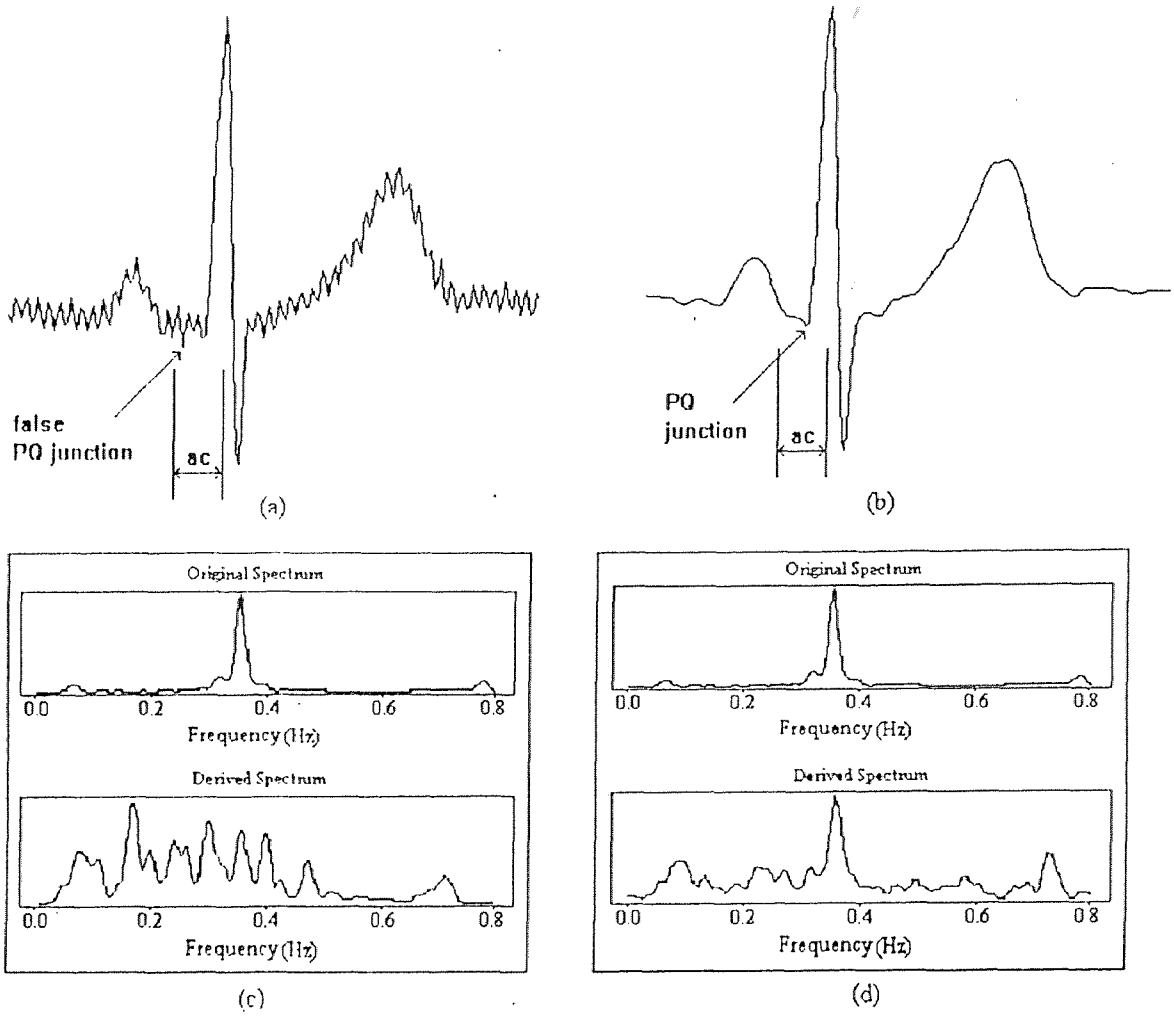

Figure 4.5 Influence of the PQ junction detection to the ECG-derived respiration spectrum. The vertical scale for the spectral graph ((c) and (d)) is arbitrary. (a) incorrect PQ junction detection due to the presence of noise; (b) correct PQ junction after the removal of noise; (c) original spectrum and false derived spectrum caused by (a); (d) original spectrum and correct derived spectrum.

that point. Due to the incorrect PQ junction detection, the derived spectrum has no association with the original spectrum as shown in Figure 4.5 (c). This problem could be overcome by using a proper smoothing technique. Figure 4.5 (b) shows the same ECG signal after smoothing, where the correct PQ junctions were detected and the true respiration information was derived (Figure 4.5 (d)). An alternative way to solve this problem is to set the time period ac as close to the expected PQ junction as possible to exclude the spikes within ac.

There is only one parameter k (see equation 2.1) which can be changed when performing the QRS area calculation. The time window length (see section 2.4.2) is determined by the average length between the PQ junction and the R peak position as well as the k value. The value of k is determined at the beginning of each data analysis by visually inspecting an ECG wave and choosing a k value to get the time window width as close to the width of the QRS complex as possible. As long as the k value is determined, there is no need to change during a data analysis. Compared to the parameters in R peak and PQ junction detection, k value selection is less critical.

4.4 Future Work

The clinical significance of heart rate variation can be understood only with reference to respiration. Our study provides a method to obtain respiration from the ECG signal when respiration information is not directly available. This can be done either directly or from a Holter recording. It is therefore possible to do spectral analysis of heart rate variability and determine the frequency of the spectral peak occurring at the respiration frequency. In future study, the following work should be performed:

(1) to collect and analyze data on abnormal subjects to verify the conclusions of the present study.

(2) to optimize the signal processing software to improve the detection and calculation accuracy and shorten the processing time.

(3) to perform cross correlation test between the original respiration and ECG-derived respiration to verify the similarity of these two time domain signals.

APPENDIX A

FIGURES OF ORIGINAL AND DERIVED RESPIRATION AND THEIR SPECTRA

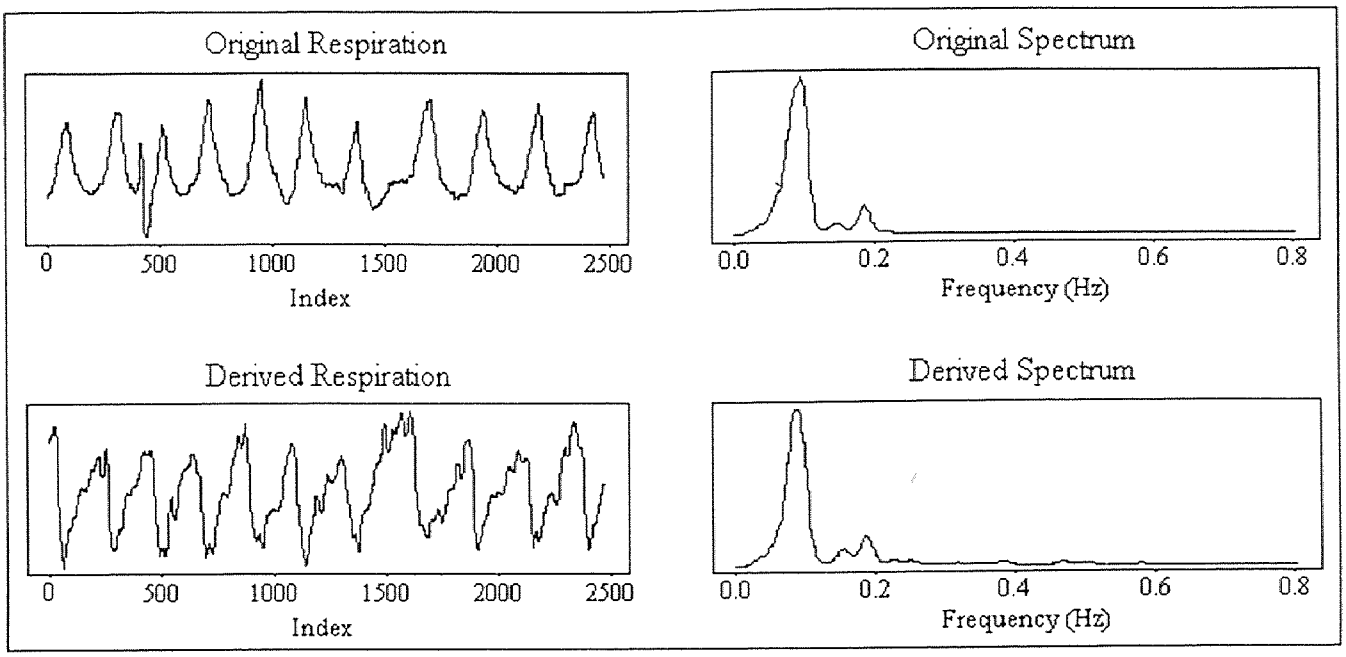

(a) Resting, non-paced breathing

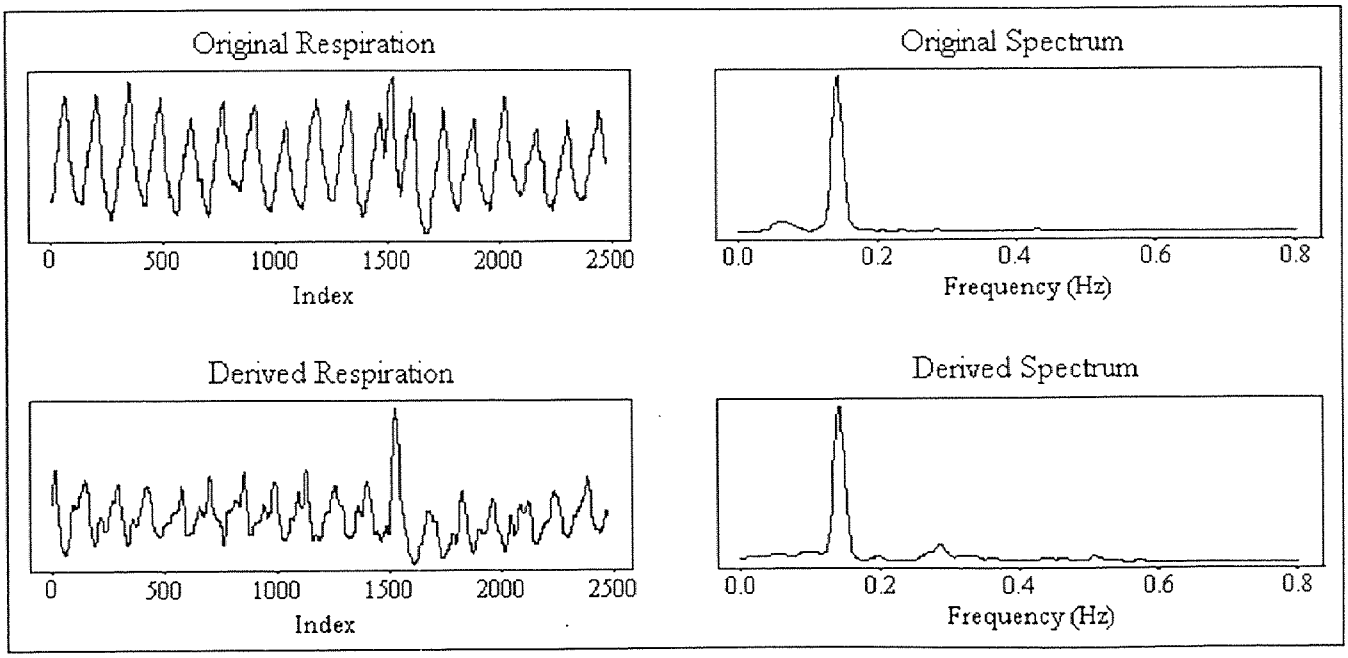

(b) Resting, paced breathing at a rate of 8 breaths per minute

Figure 3.1 Original respiration and ECG-derived respiration and their spectra. In the respiration figures (left side), the horizontal axis is time and the vertical axis is voltage. In the spectral figures (right side), the vertical axis is power density (continued on next page).

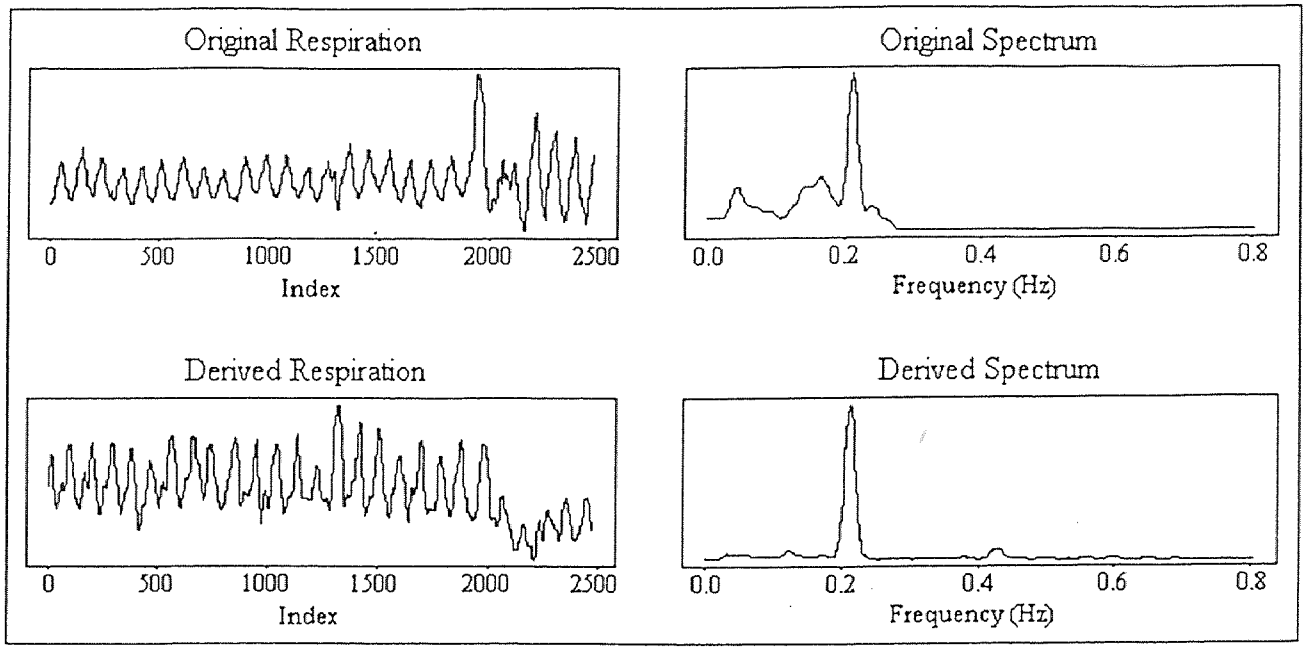

(c) Resting, paced breathing at 12 breaths per minute

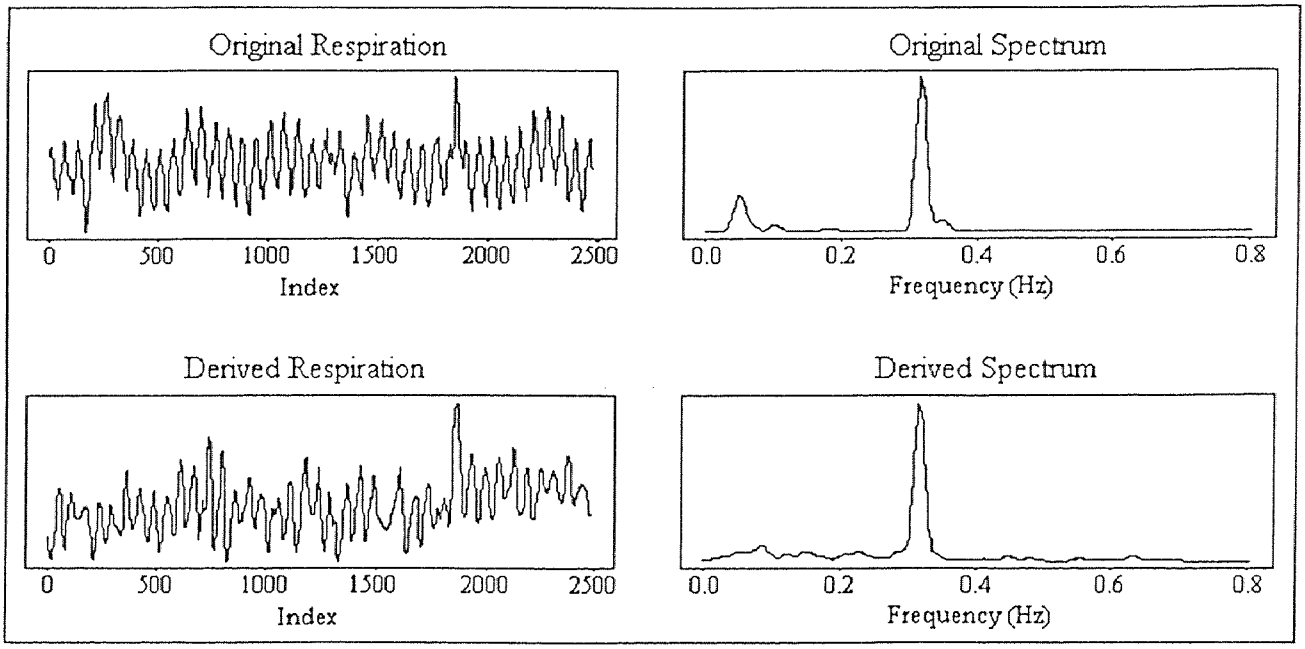

(d) Resting, paced breathing at 18 breaths per minute

Figure 3.1 (continued).

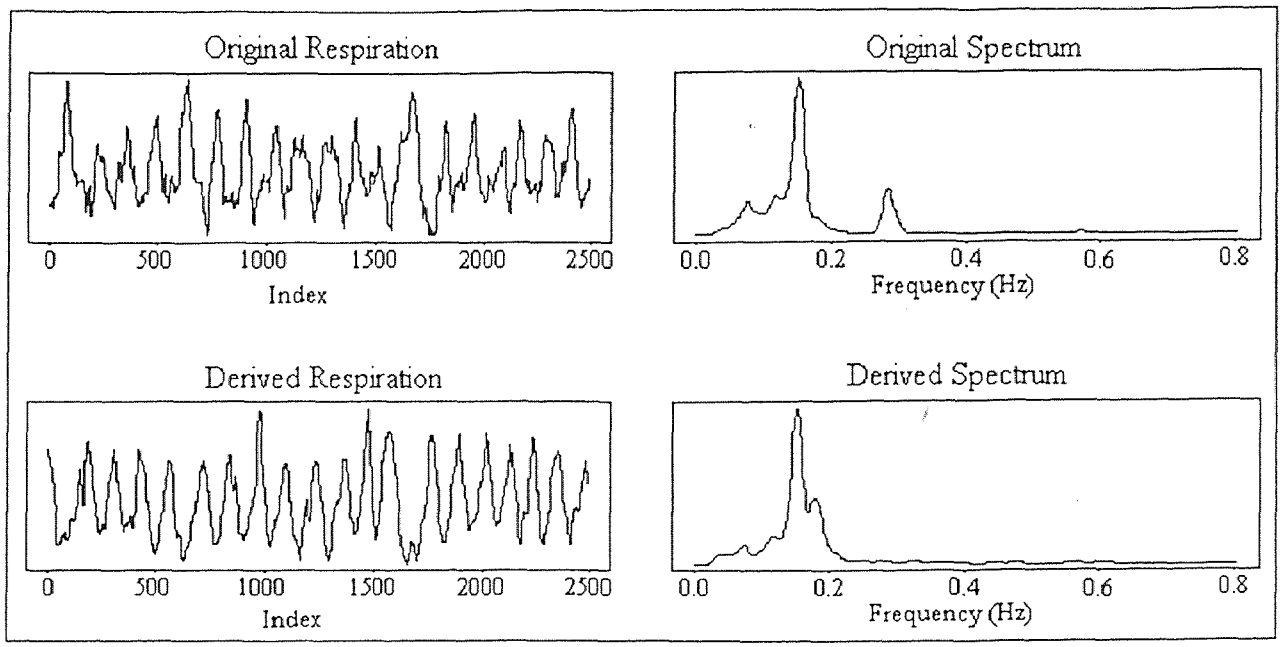

(e) Exercising at 2 METS

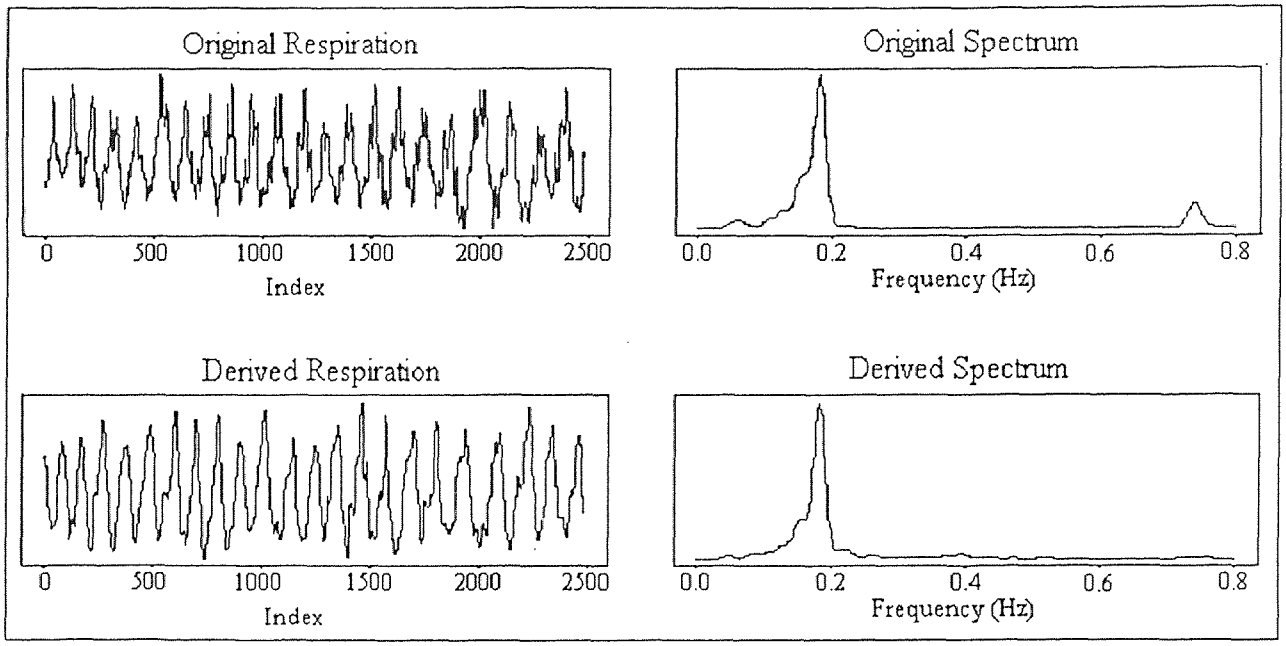

(f) Exercising at 3 METS

Figure 3.1 (continued).

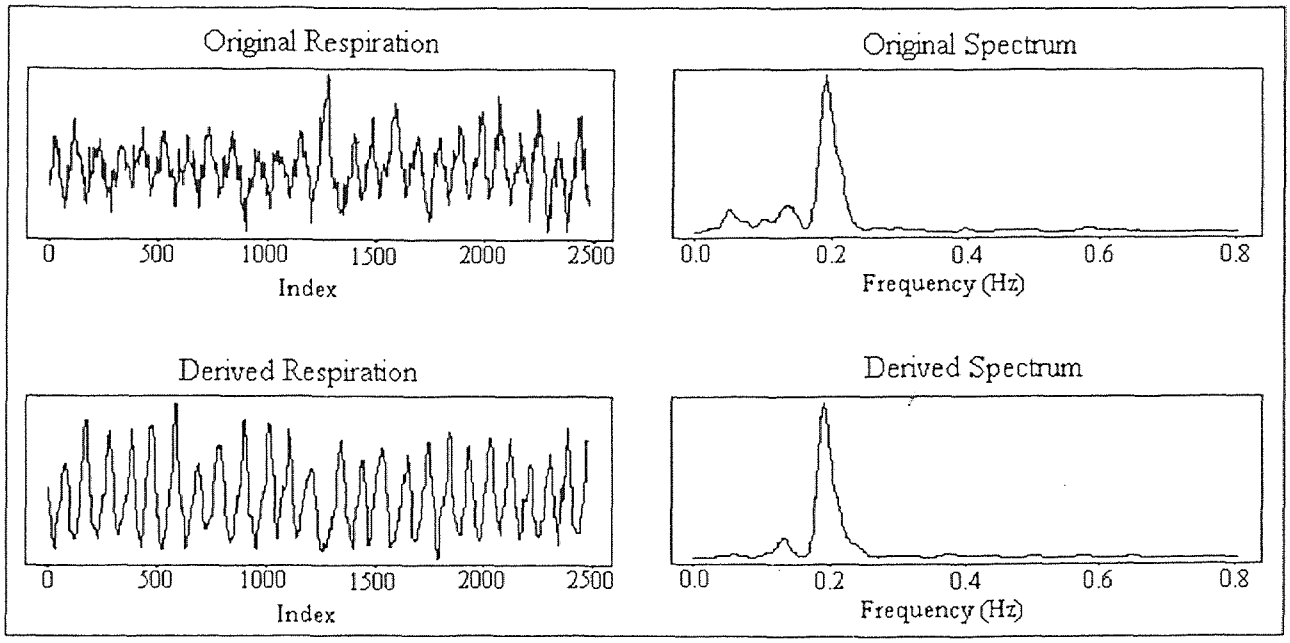

(g) Exercising at 4 METS

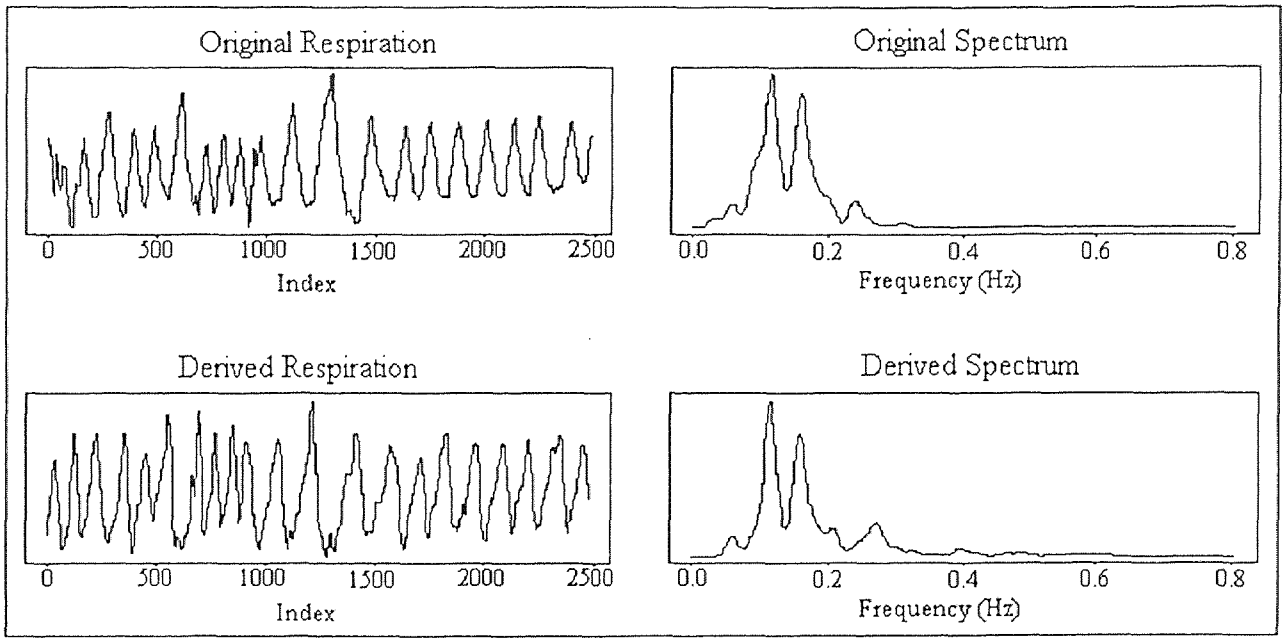

(h) Recovery, immediately following exercise

Figure 3.1 (continued).

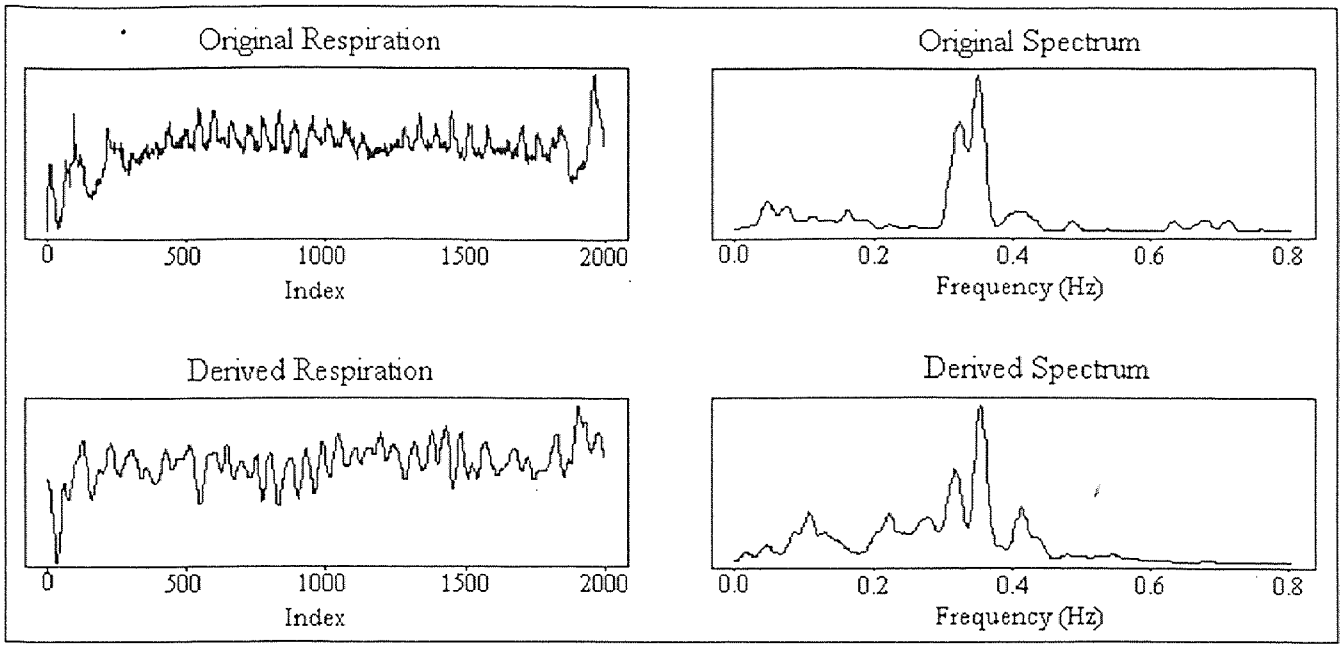

(a) Resting, non-paced breathing

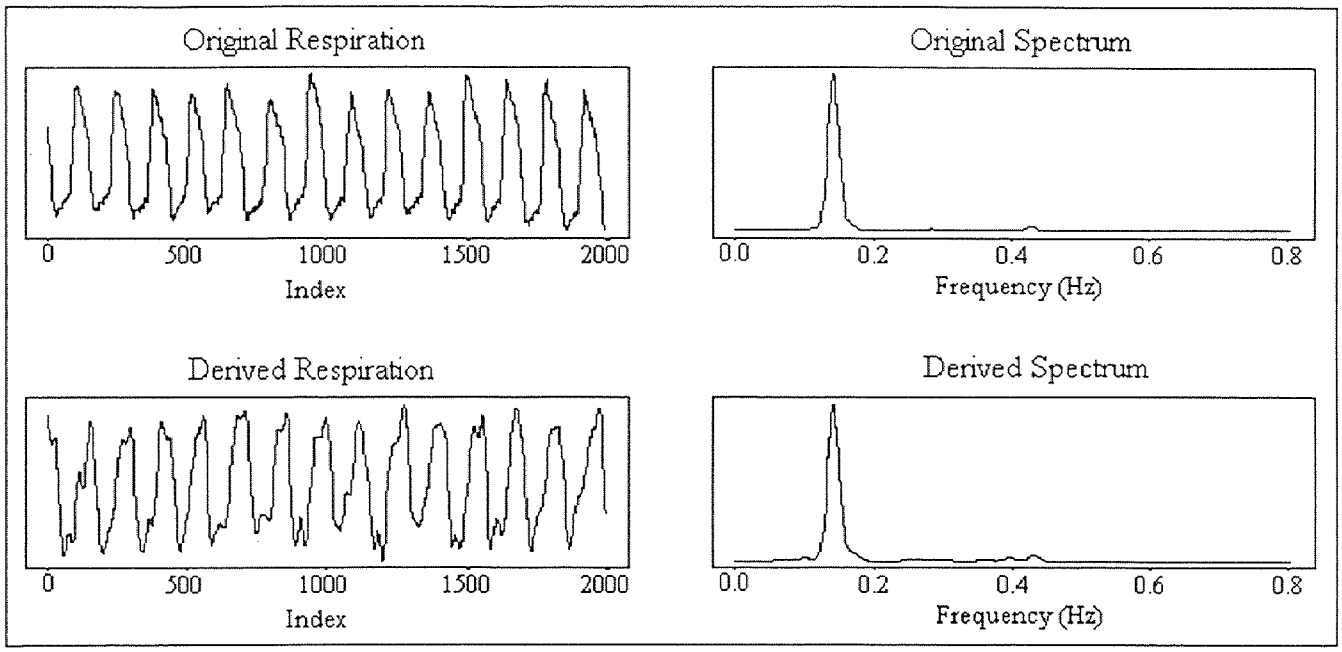

(b) Resting, paced breathing at a rate of 8 breaths per minute

Figure 3.5 Comparison of original respiration with the ECG-derived respiration and their spectra for Holter data. In the respiration figures (left side), the horizontal axis is time and the vertical axis is voltage. In the spectral figures (right side), the vertical axis is power density (continued on next page).

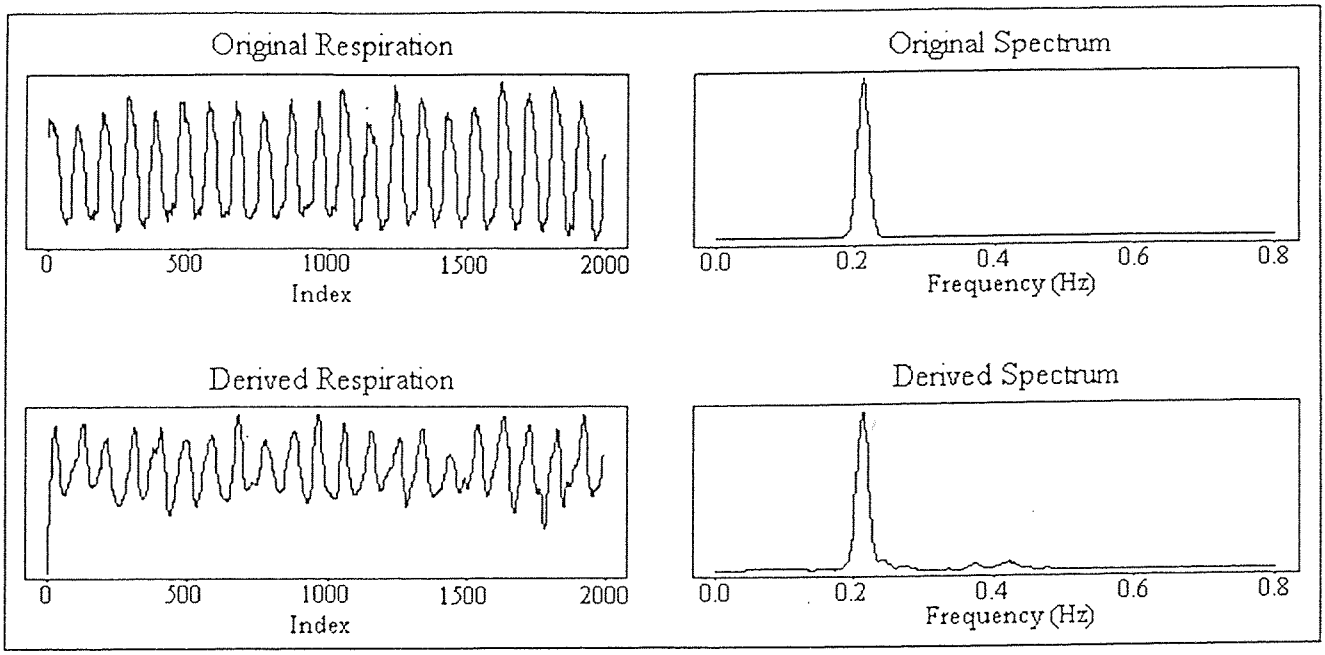

(c) Resting, paced breathing at 12 breaths per minute

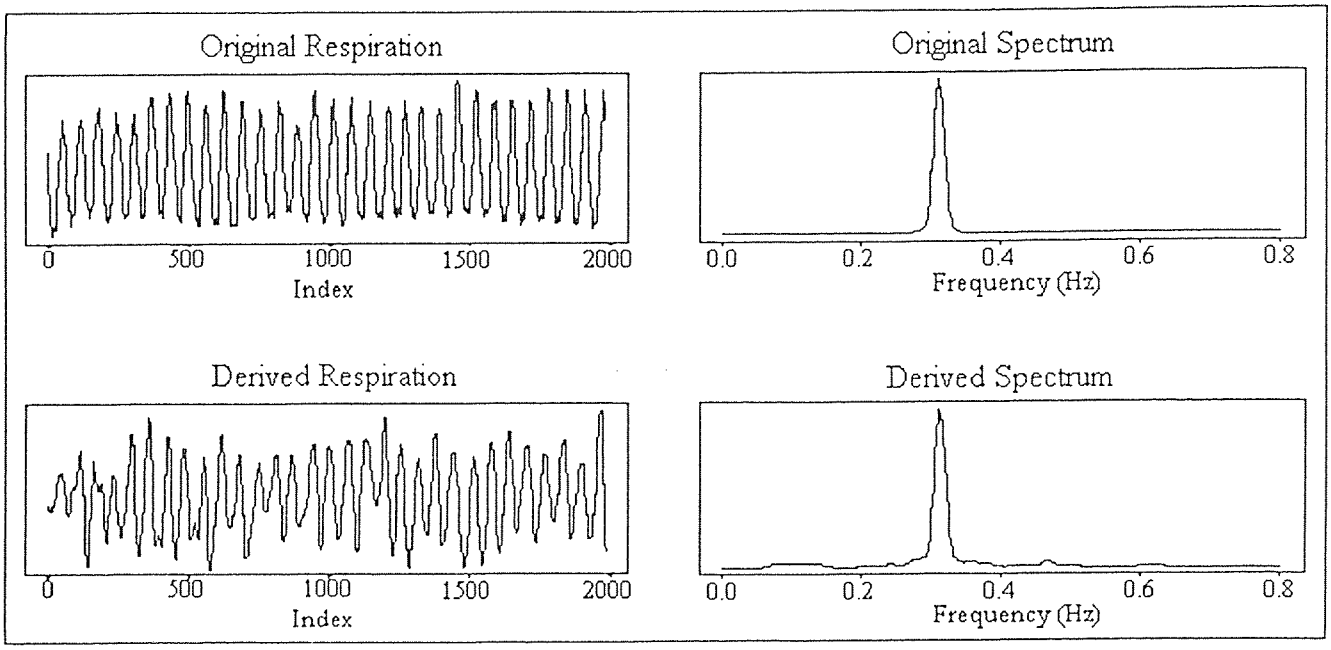

(d) Resting, paced breathing at a rate of 18 breaths per minute

Figure 3.5 (continued).

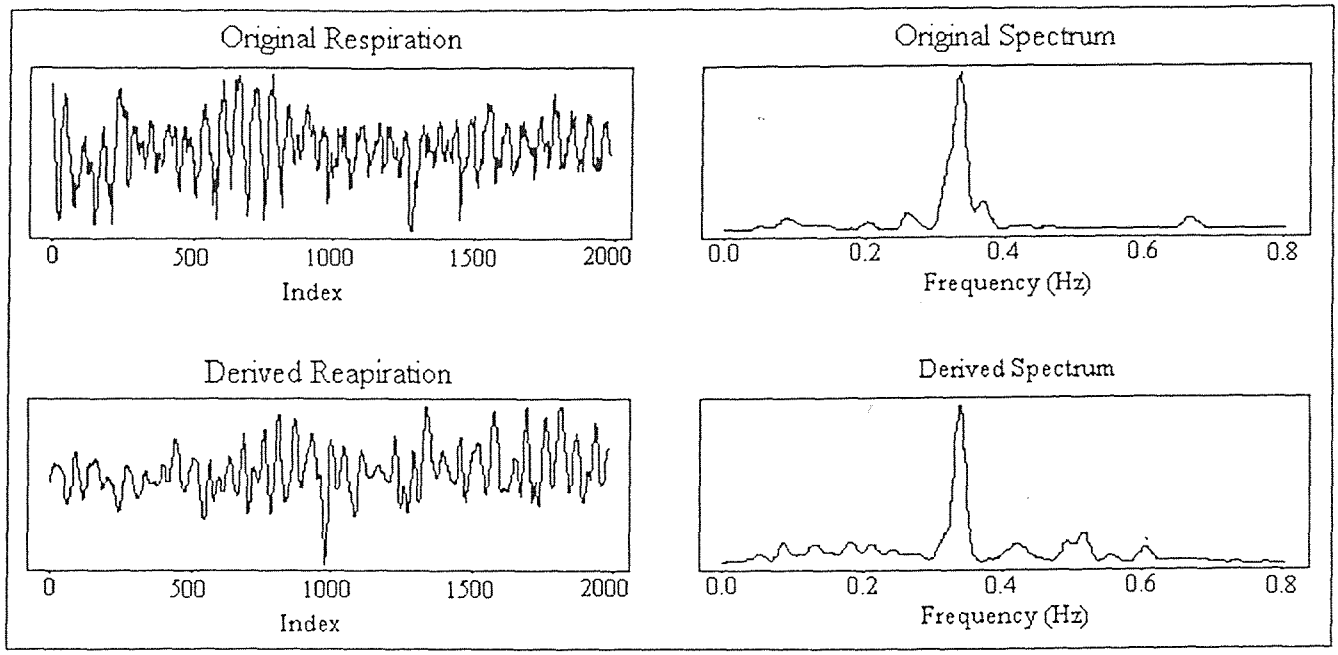

(e) Exercising at 2 METS

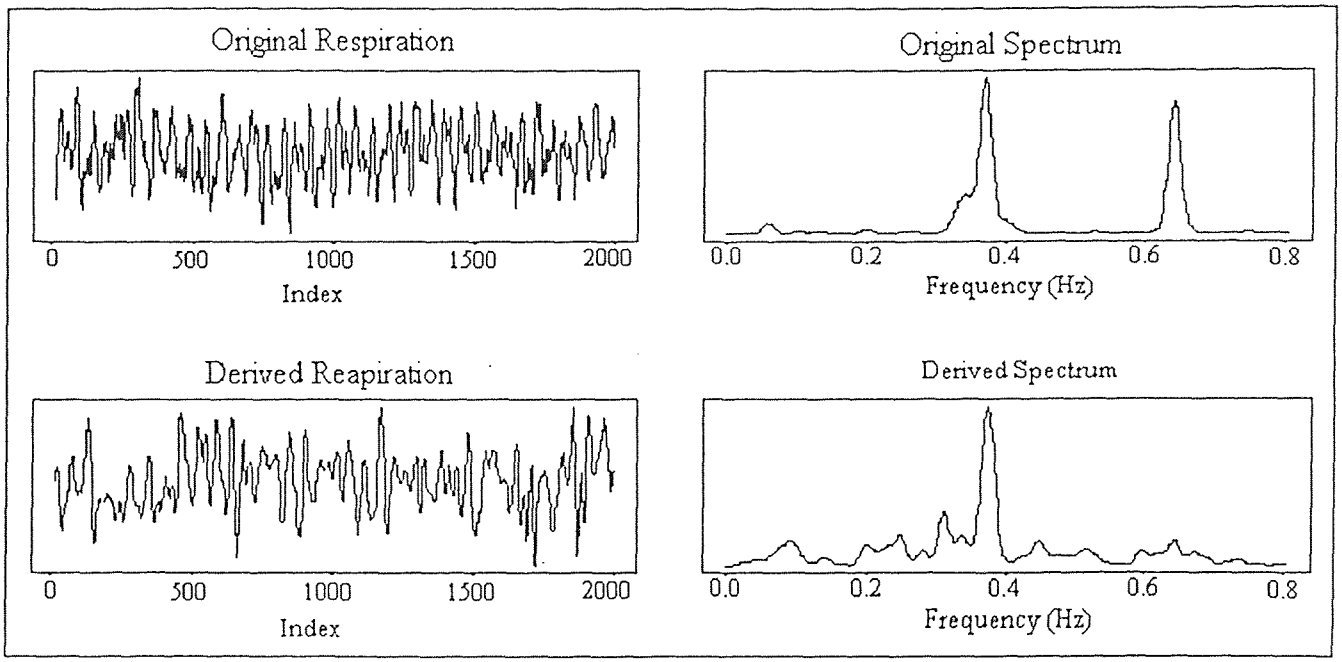

(f) Exercising at 3 METS

Figure 3.5 (continued).

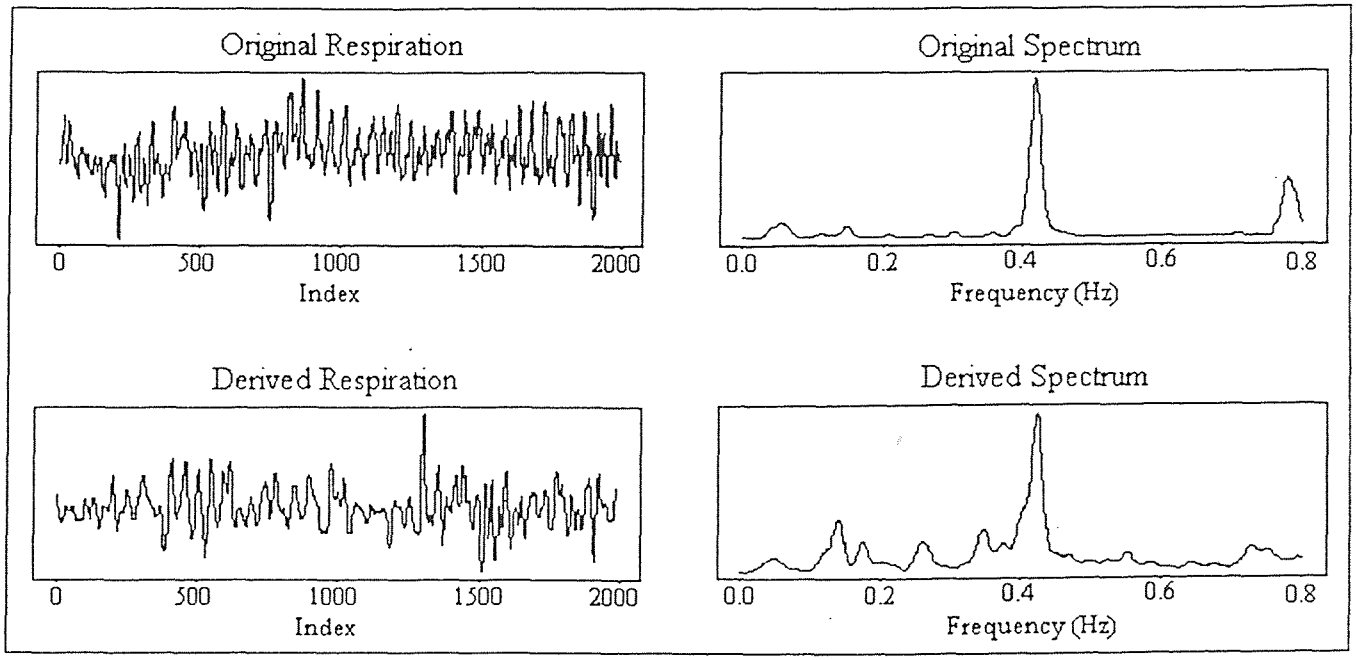

(g) Exercising at 4 METS

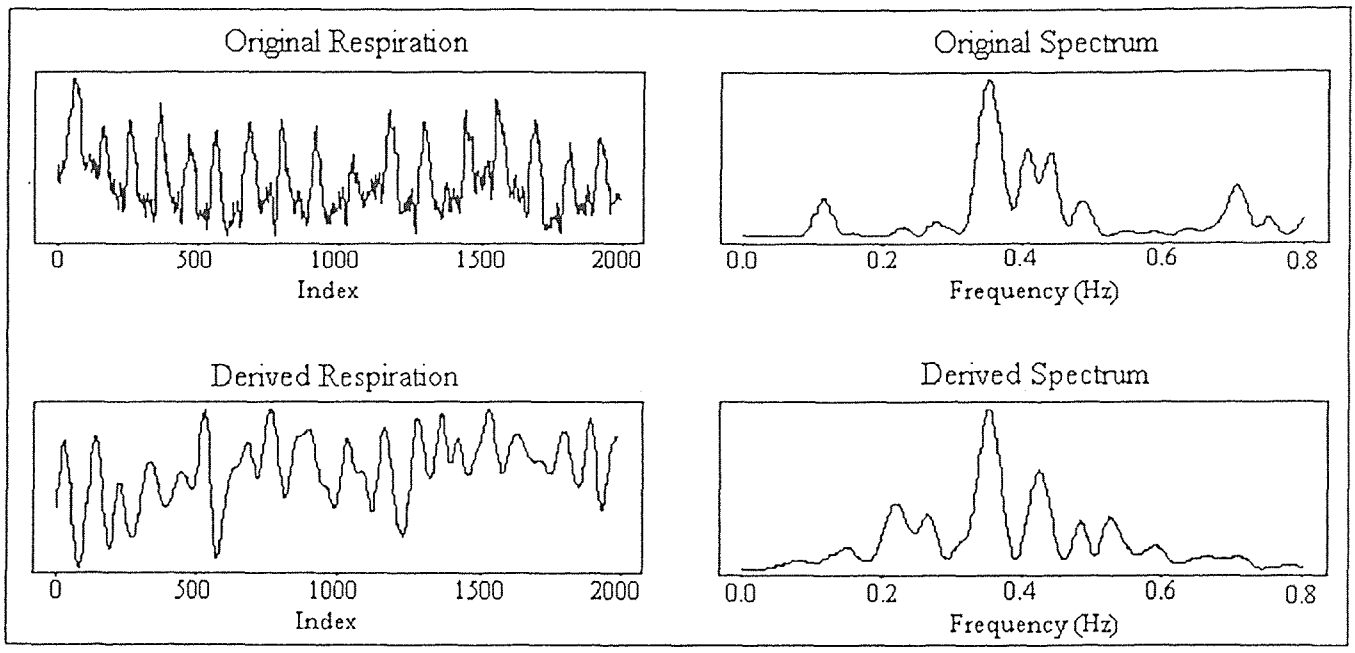

(h) Recovery, immediately following exercise

Figure 3.5 (continued).

APPENDIX B

PROCEDURE OF DERIVING RESPIRATION FROM ECG

Since we used the respiration recorded by the impedance pneumography device as our original respiration throughout the study, we processed the respiration signal using this procedure. When this original respiration is not available or only one lead ECG signal is available, the procedure should be modified properly. We will use a sample data file, r032594e, to explain the syntax of the programs. It has three columns: 1) original respiration; 2) lead I ECG; 3) lead III ECG.

A. R Peak Detection

After the acquired data are scanned in S-Plus, use FRPK to detect the lead I ECG signal. FRPK is a modified version of the peak detection part of LWS. The three parameters (qhg, mindiff, and hash) should be selected properly according the signal amplitude, noise level, and average interbeat index numbers. The syntax for FRPK is as following:

```
> r032594e.1pk_frpk (r032594e[,2])
```

where r032594e.1pk is the R peak vector generated. If miss detection is present, use FMRPK (modified version of MQRS) to detect the missed R peak manually until an R peak vector containing all R peak positions is generated.

> r032594e.mpk_fmrpk (r032594e[,2], r032594e.1pk)

If necessary, use VISCHK to inspect the detected R peak positions.

> vischk (r032594e[,2], r032594e.1pk)

B. PQ Junction Detection and QRS Area Calculation for Lead I

QRSCA is the program to detect the PQ junctions and calculate the QRS complex areas using the detected R peak positions. There two parameters (ac and k, see section 2.4 2. for detail) must be selected properly.The default values for ac and k are 7 and 2 respectively. Use the R peak vector generated from last step and lead I ECG signal to calculate the information for lead I.

> r032594e.1qr_qrsca (r032594e[,2], r032594e.1pk)

If manual R peak detection is performed in step A, the R peak vector r032594e.mpk should be used instead of using r032594e.1pk. QRSCA displays the result of the QRS area calculation automatically in a graph. The presence of the outliers of the area calculation can be inspected visually through the graph. If present, the outliers must be removed by using RMBQ.

> r032594e.rem_rmbq (r032594e.1qr)

RMBQ displays the area values graphically and allows you to remove the outliers manually by using the mouse button. Since RMBQ actually removes the R peaks corresponding to the area outliers, these suspect R peaks have to be re-detected by using FMRPK and the QRS area calculation has to be done once again. This step may be repeated more than once until there are no outliers of QRS area or the outliers are the true results of the area calculation.

C. PQ Junction Detection and QRS Area Calculation for Lead III

Use the R peak vector generated in step A or modified in step B and the lead III ECG signal to calculate the QRS complex areas for lead III. Normally, there are no more outliers in the result of the area calculation since they were removed and the R peaks were re-detected in the last step.

> r032594e.2qr_qrsca (r032594e[,3], r032594e.1pk)

Similarly, if manual R peak detection was performed in step A or area outliers removed in step B, the R peak vector used here should be the latest version instead of > r032594e.1pk.

D. Angle Calculation and Interpolation

Program DUALL calculates the angle of the cardiac electrical vector axis using the area information obtained from steps B and C. The cubic spline interpolation is performed by program EDR to produce a continuous ECG-derived respiration signal. No user selected

parameter is required in this program.

> r032594e.dr_edr (duall (r032594e.1qr, r032594e.2qr))

E. Spectrum Generation

After obtaining the derived respiration, use FSP to generate the spectrum for both the original and the derived respiration.

> r032594e.dfi_fsp (r032594e[,1], r032594e.dr)

The original and the derived respiration and their spectra are displayed by DGF.

> dgf (r032594e.dfi, title="r032594e")

F. Central Frequency Calculation

SPCP calculates the central frequencies for both the original and the derived spectra. There are three parameters h, f1, and f2. The h is the percentage of the amplitude of the spectral peak from which the low frequency f_l and high frequency f_h are calculated (see Figure 3.2). The default h is 0.3. In cases that the interference is higher than the respiration frequency peak present in the original spectrum, use f1 and f2 to exclude the interference.

> spcp (r032594e.dfi)

APPENDIX C

S-PLUS PROGRAMS

1. FRPK

```
function(x, zf = 15, mindiff = 50, qhg = 0.25, zdelta =
 0, tooruff
         = 0.8, hash = 30)
{
#x: ecg signal
        x.pk <- lwzx(x, f = zf, mindiff = mindiff, qx =
 qhg, delta
                  = zdelta, hash = hash)
        pk <- x.pk$pk
        ibi <- diff(pk)
        mruff <- max(abs(ruff(ibi)))
        if(mruff >= tooruff) {
                print(paste("IBI'S MAY BE TOO RUFF"))
                print(paste("MAX IBI IS", max(ibi), "["
, (1:length(
                        ibi))[ibi >= max(ibi)], "]"))
                print(ibi)
        }
        pk
}
```

2. FMRPK

```
function(x, qx)
{
#x: ecg data(col 2); qx: output of frpk
        xout <- pout(diff(qx))
        if(length(xout$high) == 0) {
                qfx <- list(qx = qx, ibi = diff(qx))
                return(qfx)
                stop()
        }
        print("bracket missing peaks using mouse", quot
e = F)
        cx <- vector("numeric", 0)
        print(xout$high)
        for(i in xout$high[1:length(xout$high)]) {
                i1 <- i - 2
                i2 <- i + 2
                if(i1 < 1)
                        i1 <- 1
                if(i2 > length(qx))
                        i2 <- length(qx)
                plot(qx[i1]:qx[i2], x[qx[i1]:qx[i2]], t
ype = "l")
                abline(v = qx[(i1):(i2)])
                bx <- locator()$x
                if(length(bx) > 0) {
                        if(length(bx) > 2) {
                                bx <- unique(bx)
                        }
                        if(length(bx) %% 2 > 0) {
                                bx <- bx[1:(length(bx)
- (length(
                                  bx) %% 2))]
                        }
                        for(j in seq(1, length(bx), 2))
 {
                                bb <- floor(bx[j])
                                be <- ceiling(bx[j + 1]
)
                                tx <- order(x[bb:be])[1
ength(bb:be
```

```
                                        )] + bb
                                    abline(v = tx, lty = 2)
                                    cx <- c(cx, tx)
                            }
                    }
            }
            print(cx)
            for(i in 1:length(cx)) {
                    qxu <- qx[qx < cx[i]]
                    qxo <- qx[qx > cx[i]]
                    qx <- c(qxu, cx[i], qxo)
                    print(length(qx))
            }
#qfx <- list(qx = qx, ibi=diff(qx))
            qfx <- qx
            qfx
}
```

3.QRSCA

```
function(x, pkx, ac = 7, k = 2)
{
#x:ecg data(col 2), pkx: R peak, hwin:
        hwin_ac
        if(pkx[1] < hwin) {
                pkx <- pkx[2:length(pkx)]
        }
        if(length(x) < (pkx[length(pkx)] + 3 * hwin)) {
                pkx <- pkx[1:(length(pkx) - 1)]
        }
        lwf <- lowess(1:length(x), x, f = 45/length(x),
 iter = 2,
                delta = 0.1)$y
        x <- x - lwf
        minx <- vector("numeric", 0)
        for(i in 1:length(pkx)) {
                minx1 <- ((pkx[i] - hwin):pkx[i])[(x[(p
kx[i] -
                        hwin):pkx[i]]) <= min(x[(pkx[i]
 - hwin):
                        pkx[i]])]
                if(length(minx1) > 1) {
                        minx1 <- minx1[length(minx1)]
                }
                minx <- c(minx, minx1)
        }
        if(length(pkx) != length(minx)) {
                print(paste("Number of Q's is not equal
 to that of R's"
                        ))
                print(paste("Q's:", length(minx)))
                print(paste("R's:", length(pkx)))
                stop()
        }
        shwd <- round(mean(pkx - minx) * k)
        qrsca <- vector("numeric", 0)
        for(i in 1:length(minx)) {
                cols <- x[(minx[i] + 1):(minx[i] + shwd
)]
                ca1 <- sum(cols)
```

```
                dft <- x[minx[i]] * shwd
                rca <- cal - dft
                qrsca <- c(qrsca, rca)
        }
        par(mfrow = c(1, 1))
        plot(qrsca)
        z <- list(qrsca = qrsca, pkx = pkx, x = x, minx
 = minx)
        z
}
```

4. RMBQ

```
function(x)
{
#x:output of qrsca
        x1 <- x$qrsca
        x2 <- x$pkx
        plot(x1)
        xs <- 1:length(x1)
        bqa <- identify(xs, x1, plot = T)
        j <- 0
        for(i in 1:length(bqa)) {
                x2 <- x2[ - (bqa[i] - j)]
                j <- j + 1
        }
        x2
}
```

5. DUALL

```
function(x1, x2)
{
#x1:first lead qrsca;x2:second lead qrsca
        qca1 <- x1$qrsca
        qca2 <- x2$qrsca
        qrsca <- atan(qca1/qca2)
        z <- list(qrsca = qrsca, pkx = x1$pkx)
        z
}
```

6. EDR

```
function(x)
{
# x: output of qrsca
        pkx <- x$pkx
        qrsca <- x$qrsca
        n <- pkx[length(pkx)] - pkx[1] + 1
        iedr <- spline(pkx, qrsca, n)
        sted <- c(iedr$x[1], iedr$x[length(iedr$x)])
        z <- list(iedr = iedr$y, sted = sted)
        z
}
```

7. FSP

```
function(x1, x2, title = "", f2 = 0.2)
{
#x1: resp signal; x2: edr output
        orresp <- x1
        edresp <- x2$iedr
        stp <- x2$sted[1]
        edp <- x2$sted[2]
        orresp <- orresp[stp:edp]
        d.orp <- orresp[seq(1, length(orresp), 10)]
        d.orpl <- lowess(1:length(d.orp), d.orp, f = 0.
3, iter = 2,
                delta = ceiling((length(d.orp) * 0.3)/8
))$y
        d.orps <- spect(d.orp - d.orpl, nt = 8192, ns =
 6)
        d.edr <- edresp[seq(1, length(edresp), 10)]
        d.edrl <- lowess(1:length(d.edr), d.edr, f = f2
, iter = 2,
                delta = ceiling((length(d.edr) * 0.3)/8
))$y
        d.edrs <- spect(d.edr - d.edrl, nt = 8192, ns =
 6)
        z <- list(d.orp = d.orp, d.edr = d.edr, d.orps
= d.orps[1:
                330], d.edrs = d.edrs[1:330])
        z
}
```

8. DGF

```
function(x, title = "")
{
#x: output if fsp
        d.orp <- x$d.orp
        d.edr <- x$d.edr
        d.orps <- x$d.orps
        d.edrs <- x$d.edrs
        xf <- ((1:330) - 1)/8192 * 20
        dev.set(which = 2)
        par(mfrow = c(2, 1), mar = c(4, 5, 3, 1))
        plot(d.orp, type = "l", main = paste(title, "-O
riginal"))
        plot(d.edr, type = "l", main = paste(title, "-D
erivation")
                )
        dev.set(which = 3)
        par(mfrow = c(2, 1), mar = c(4, 5, 3, 1))
        plot(xf, d.orps[1:330], type = "l", xlab = "Fre
quency(Hz)",
                ylab = "Power", main = paste(title, "-O
riginal"))
        plot(xf, d.edrs[1:330], type = "l", xlab = "Fre
quency(Hz)",
                ylab = "Power", main = paste(title, "-D
erivation")
                )
}
```

9.SPCP

```
function(x, h = 0.3, nt = 8192, sr = 20, f1 = 1, f2 = 1
00)
{
#x:output of fsp
        fn <- sr/(nt * 3)
        x1 <- x$d.orps
        x2 <- x$d.edrs
        xscal <- 1:330
        x1 <- spline(xscal, x1)$y
        x2 <- spline(xscal, x2)$y
        f1 <- round(length(x1) * (f1/100))
        f2 <- round(length(x1) * (f2/100))
        x1.c <- x1[f1:f2]
        x2.c <- x2[f1:f2]
        x1.mc <- (1:length(x1.c))[(x1.c >= max(x1.c))]
        x2.mc <- (1:length(x2.c))[(x2.c >= max(x2.c))]
        x1.m <- x1.mc + f1 - 1
        x2.m <- x2.mc + f1 - 1
        x11.r <- rev(x1[1:x1.m])
        x12 <- x1[x1.m:length(x1)]
        x21.r <- rev(x2[1:x2.m])
        x22 <- x2[x2.m:length(x2)]
        f1.lr <- fm1(x11.r, x1[x1.m] * h)
        f1.l <- x1.m - f1.lr + 1
        f1.hm <- fm1(x12, x1[x1.m] * h)
        f1.h <- x1.m + f1.hm - 1
        f2.lr <- fm1(x21.r, x2[x2.m] * h)
        f2.l <- x2.m - f2.lr + 1
        f2.hm <- fm1(x22, x2[x2.m] * h)
        f2.h <- x2.m + f2.hm - 1
        a1 <- sum(x1[f1.l:(f1.h - 1)])
        a2 <- sum(x2[f2.l:(f2.h - 1)])
        ai.1 <- a1/(x1[x1.m] * (f1.h - f1.l))
        ai.2 <- a2/(x2[x2.m] * (f2.h - f2.l))
        ha1.sm <- x1[f1.l]
        for(i in (f1.l + 1):f1.h) {
                ha1 <- x1[i]
                ha1.sm <- sum(ha1.sm, ha1)
                if(ha1.sm >= (a1/2)) {
                        cf1 <- (1:length(x1))[(x1 == x1
```

```
[i])]
                        break
                }
        }
        ha2.sm <- x2[f2.l]
        for(i in (f2.l + 1):f2.h) {
                ha2.sm <- sum(ha2.sm, x2[i])
                if(ha2.sm >= a2/2) {
                        cf2 <- (1:length(x2))[(x2 == x2
[i])]
                        break
                }
        }
        z <- list(f1 = c(f1.l, f1.h, cf1) * fn, f2 = c(
f2.l, f2.h,
                cf2) * fn, ra = c(ai.1, ai.2))
        z
}
```

REFERENCES

1. Wartak, J. 1970. *Simplified Vectorcardiography.* Philadelphia: J. B. Lippincott Company.

2. Berne, R. M., and M. N. Levy. 1988. *Physiology.* St. Louis: The C.V. Mosby Company.

3. Goldberger, A. L., D. R. Rigney, and B. J. West. 1990. "Chaos and Fractals In Human Physiology." *Scientific American.* 262: 42-49.

4. DeMeersman, R. E. 1993. "Aging as a modulator of respiratory sinus arrhythmia." *Journal of Gerontology: Biological Sciences.* 48(2): B74-B78.

5. Kitney, R. I., T. Fulton, A. H. McDonald, and D. A. Linkens. 1985. "Transient interactions between blood pressure, respiration and heart rate in man." *Journal of Biomedical Engineering.* 7: 217-225.

6. Kitney, R. I., and O. Rompelman. 1980. *The study of heart rate variability.* Oxford: Clarendon.

7. Hayano, J., Y. Sakakibara, M. Yamada, T. Kamiya, T. Fujinami, K. YokoYama, Y. Watanabe, and K. Takata. 1990. "Diurnal variations in vagal and sympathetic cardiac control." *American Journal of Physiology.* 258: H642-H646.

8. Kitney, R. I. 1975. "An analysis of the nonlinear behavior of the human thermal vasomotor control system." *Journal of Theoretical Biology.* 52: 231-248.

9. Bigger, J. T., J. L. Fleiss, R. C. Steinman, L. M. Rolnitzky, R. E. Kleiger, and J. N. Rottman. 1992. "Frequency domain measures of heart period variability and mortality after myocardial infarction." *Circulation.* 85(1): 164-171.

10. Berntwon, G. G., J. T. Cacioppo, and K. S. Quigley. 1993. "Respiratory sinus arrhythmia: Autonomic origins, physiological mechanisms, and psychophysiological implications." *Psychophysiology.* 30: 183-196.

11. Shin, S. J., W. N. Tapp, S. S. Reisman, and B. H. Natelson. 1989. "Assessment of autonomic regulation of heart rate variability by the method of complex demodulation." *IEEE Transactions on Biomedical Engineering.* 36(2):274-282.

12. Guyton, C. 1991. *Textbook of Medical Physiology.* Philadelphia: W. B. Saunders Company.

13. DeBoer, R. W., J. W. Karemaker, and J. Strackee. 1987. "Hemodynamic fluctuations and baroreflex sensitivity in humans: a beat-to-beat model." *American Journal of Physiology*. 253: H680-H687.

14. Saul, J. P., R. D. Berger, and R. J. Cohen. 1990. "Short term blood pressure regulation: a combination of feedback and mechanics (Abstract)." *Proc. Annu. Int. Conf. IEEE Eng. Med. Biol. Soc.* 12: 2.

15. Daly, M. B., and E. Kirkman. 1989. "Differential modulation by pulmonary stretch afferents of some reflex cardioinhibitory responses in the cat." *Journal of Physiology*. 417: 323-341.

16. Novak, V., P. Novak, J. D. Champlain, A. R. Blanc, R. Martin, and R. Nadeau. 1993. "Influence of respiration on heart rate and blood pressure fluctuations." *Journal of Applied Physiology*. 74(2): 617-626.

17. Akselrod, S., D. Gordon, J. B. Madwed, N. C. Snidman, D. C. Shannon, and R. J. Cohen. 1985. "Hemodynamic regulation: investigation by spectral analysis." *American Journal of Physiology*. 249: H867-H875.

18. Zhang, P. Z., S. S. Reisman, and W. N. Tapp. 1992. "Heart rate variability study using phase response curve." *14th IEEE Conference of Biomedical Engineering*. 2: 571-572.

19. Pinciroli, F., R. Rossi, and L. Vergani. 1985. "Detection of electrical axis variation for the extraction of respiratory information." *Computers in Cardiology*. 12: 499-502.

20. Moody, G. B., R. Mark, A. Zoccola, and S. Mantero. 1985. "Derivation of respiratory signals from multi-lead ECGs." *Computers in Cardiology*. 12: 113-116.

21. Moody, G. B., R. G. Mark, M. A. Bump, J. S. Weinstein, A. D. Berman, J. E. Mietus, and A. L. Goldberger. 1986. "Clinical validation of the ECG-derived respiration (EDR) technique." *Computers in Cardiology*. 13: 507-510.

22. Ganong, W. F. 1993. *Review of Medical Physiology*. New York: Appleton & Lange.